Master Dissertation of Jaeyong Kim

Analysis of Effect on Damping Ratio by Operating Conditions of Generators

발전기의 운전조건에 따른 감쇠비의 영향 분석

February 2017

Jaeyong Kim

Electrical Engineering Major
Department of Electrical Engineering
and Computer Science

Graduate School of Engineering
Seoul National University

Analysis of Effect on Damping Ratio by Operating Conditions of Generators

Jaeyong Kim

Submitting a Master Dissertation
of Electrical Engineering

February 2017

Jaeyong Kim

Electrical Engineering Major

Department of Electrical Engineering
and Computer Science
Graduate School of Engineering
Seoul National University

Research Advisor: Jong-Keun Park

Confirming Master Dissertation written by

Jaeyong Kim

February 2017

Chair: Seung-Il Moon (Seal)

Vice Chair: Jong-Keun Park (Seal)

Examiner: Yong Tae Yoon (Seal)

Abstract

Analysis of Effect on Damping Ratio by Operating Conditions of Generators

Jaeyong Kim

Department of Electrical Engineering and Computer Science

The Graduate School of Engineering

Seoul National University

Constant small fluctuations in loads or generation may cause small disturbances in power system. The rotor angle will oscillate around the equilibrium point to move to the steady state following small disturbances. If this oscillation cannot be suppressed due to insufficient damping, the magnitude of electromechanical oscillation will increase continuously, causing a loss of synchronism in power system. Today's practical power systems, small disturbances mostly arise from insufficient damping of system oscillation. Hence, this signifies the importance of improving damping effectively. Accordingly, this paper investigates the effect of operating condition of a generator on damping ratio through the theoretical analysis and the case studies thereof.

Small signal stability is the ability of the power system to maintain the synchronism under the small perturbations. The analysis of the small

signal stability is essential to examine the effect of small disturbances on power system. To begin with, it is necessary to understand the dynamics of a synchronous machine. The equations thereof can be derived from the swing equation which can be transformed into a state space formula containing a state matrix after the linearization. The eigenvalue and damping ratio are determined by this state matrix, and they will be used as inputs to the modal analysis technique to perform small signal analysis.

Meanwhile, the capability of a synchronous generator is modeled with the curve formed using the maximum and minimum limits of real and reactive power output so that it can operate safely without overheating. Accordingly, the points located within this capability curve are the range of safe operating points of a generator. The operating condition of a generator is indicated as leading, lagging or unity power factor according to the location of the operating point.

The formulae for synchronizing and damping torque coefficients are expressed in terms of real and reactive power in order to reveal the relationship between these coefficients and operating conditions. The equation for infinite bus voltage, which is essential to evaluate the synchronizing and damping torque coefficients, is derived from the voltage equation of simple network system. Thereby, the mathematical linear relation between damping ratio and synchronizing and damping torque coefficients are examined. The rise of synchronizing torque coefficient brings about an increase in undamped natural frequency, while the rise in damping torque coefficient causes an increase in damping.

The effects of operating condition of a generator on damping were simulated with simple network model using PSS/E software. Then the analysis has been expanded to the real-world power system in Persian Gulf area. The specific generating units were selected and used for the theory validation and small signal stability analysis. The eigenvalues were evaluated and then the damping ratios were plotted on a complex s-plane. The theoretical model has been validated through the simulations since the damping ratio was improved as operating condition of generators moves from leading via unity to lagging. Most of the modes were located in a secure region, thereby it is satisfied the condition for ensuring the small signal stability in power systems. Through the simulations, it is proved that the operating condition should be considered with the performance of controllers for better damping.

In this paper, the effect of operating condition of a generator on damping ratio is assessed. The theoretical formulae for damping ratio and the simulation results of case study showed that the damping ratio is affected by the change in operating condition. Therefore, performance of controllers and operating conditions are both important factors to be considered for the improvement of damping ratio in power systems.

Keywords: Damping Ratio, Small Signal Stability, Operating Condition, Damping Torque Coefficient, Synchronizing Torque Coefficient, Reactive Capability Curve

Student ID Number: 2015-20906

Table of Contents

List of Figures

List of Tables

Chapter 1. Introduction

1.1. Study Background

The major function of an electric power system is to provide electricity to its customers efficiently and with assurance of stability and quality. [1] The fundamental feature of power quality is the reliability of power system, and it is the primary concern to the power system planners for the generation expansion planning. However, this has become a significant challenge in modern power network due to the uncertainty of forced outage rates (FORs) including shutdown condition of power stations and transmission or distribution lines.

Reliability is [2] the ability of power system to perform its function properly. It is defined as “the degree to which the performance of the elements of a certain system results in power being delivered to consumers within accepted standards and in the amount desired.” by NERC (The North American Electric Reliability Corporation), the organization that supervises and regulates the reliability of the North American electrical power grids.

Reliability of power system can be resolved into three categories: adequacy, operating reliability and stability. [1] In this regard, this paper will mainly focus on stability. Stability of power system is the ability of an electric power system to regain a state of operating equilibrium after being

subjected to a physical disturbance so that practically the entire system remains intact, according to Kundur et al. [3] Unfortunately in the history, stability issues with the interconnected large power networks such as rotor angle, frequency and voltage issues were revealed and got more pronounced due to several times of great blackouts.

The ability of power system to maintain 'synchronism' between machines within the system is one of the primary concern in power system stability analysis. The major components of power system stability are rotor angle (δ), power-rotor angle ($P-\delta$) relationship, and rotor speed (ω_r). Rotor angle, in its essence, indicates the angle between the q axis - the internal voltage axis ($\tilde{E}_q$) and the terminal voltage phase ($\tilde{E}_t$). Rotor angle instability occurs when there is a loss of synchronism at one or more synchronous generators.

Power systems are subjected to a wide range of small and large disturbances. Small disturbances in the form of load changes occur continually in power system; the system must be able to adjust to the changing conditions and operate satisfactorily. It must also be able to survive numerous disturbances from a severe nature, such as a short circuit on a transmission line or loss of a large generator. [3]

As its name stands for, "small signal stability" is the study on system response to small disturbances in stability analysis of power networks. These small disturbances result in synchronism issue from rotor angle separation of a generator or oscillation issue due to insufficient

damping of oscillations. These disturbances will occur persistently and inevitably in power system. However, if these will not be resolved properly and sustained, instability problem may be occurred in power system. It is crucial to improve damping in power system, since insufficient damping of oscillations will cause small disturbances and ultimately lead to the instability of power system.

1.2. Previous Studies

It was discovered that synchronous generators with Power System Stabilizer (PSS) can provide sufficient damping to transfer more power. [4] In order to improve the system stability of power system, therefore, PSS is employed. [5] Obviously, many studies have focused on the influence, tuning, performance, and design of PSS controllers to improve damping ratio for the system stability.

The function of PSS is to add damping to the oscillations of generators by controlling its excitation by using auxiliary stabilizing signals. The general input signal of PSS is the rotor speed deviation ($\Delta\omega_r$), and the amount of damping is determined by PSS gain (K_{PSS}). The following first-order lead-lag compensators compensate the phase lag between the excitation model and the synchronous machine. The output signal of PSS damps out the low frequency oscillations of power system. The effect on damping ratio may be analyzed by modal analysis technique, and it can be validated with case studies thereof. [6]

In order to increase the damping in power system, PSS are tuned mainly through its parameters of PSS gain and lead-lag compensator, and it can be done by optimization programs. The main reasons to tune PSS parameters are to compensate for the phase lag and to provide with electrical torque in phase with speed via the excitation system and generator. [7] For the optimal tuning of PSS parameters to improve damping, so far

many algorithms have been suggested including PSO (Particle Swarm Optimization) algorithm which is based on exchanging information among the particles in a network. [8]

In tuning of PSS gain, the bigger gain the faster damping of oscillations as increasing damping torque, however if the gain is too big, then the system could become unstable in controller mode. The optimal PSS gain, therefore, should be determined so that the system is stable both in controller and local mode. To do this, optimal gain should be determined as the value that has same damping ratio in both modes. Damping ratio depends on the operating condition of a generator, as a result, the PSS gain also affected by the operating condition of a generator. Even though the parameters of controllers such as AVR and PSS are affected by the operating condition of a generator, they were given as constants or estimated through the complicated process, and it is hard to find the previous literatures that consider the operating condition for improving damping in power system.

Meanwhile, the damping ratio was evaluated by computing eigenvalues for the analysis of small signal stability. Damping ratio can be expressed as a function of synchronizing torque coefficient (K_s) and damping torque coefficient (K_D). However, in many previous studies the damping torque coefficient is fixed, estimated, or simply given to evaluate damping ratio. [9, 10] The method of estimation for damping torque coefficient is not simple at all, moreover, the coefficient can be varied

according to the operation conditions. For instance, in a thesis [11], the author demonstrated how to evaluate damping ratio by varying the values of real and reactive power with only three operating conditions such as nominal operating condition, light operating condition and heavy operating condition. Likewise, many previous studies have exposed the limitation in evaluating damping ratio by fixing or estimating damping torque coefficient.

1.3. Dissertation Objective

Even though in a thesis [11], the damping torque coefficient was estimated, the values of real and reactive power were arbitrarily determined based on the severity of operating condition of a generator. It is suggested that the operating condition can be determined, in this dissertation, in the range of operating points that can generate maximum power output between leading and lagging power factor according to the specification of a generator along the reactive capability curve.

Thereby, in this thesis, the damping torque coefficient is expressed as a function of parameters of a generator such as transient and sub-transient reactance, time constant, and the angle difference between the transient emf and infinite bus. It is confirmed that the correlation between operating conditions and coefficients, K_S and K_D by expressing both synchronizing torque coefficient and damping torque coefficient as a function of real and reactive power. As it is mentioned earlier, the damping ratio is the function of synchronizing and damping torque coefficient. Therefore, the effect of damping ratio by operating condition of a synchronous generator can be established as a form of equation mathematically.

Based on the correlation among operating condition, synchronizing and damping torque coefficient, and damping ratio by the theoretical study, a practical approach for their relationship and the effect on damping of operating condition was conducted by the simulations using

PSS/E and NEVA so as to verify that whether the result of simulations matches with the mathematical theory or not. First, it is demonstrated the evaluation of damping ratio in a simple network which is composed of a generator, an infinite bus, a transformer, and transmission line connect them each other. Then, the simulation has been so expanded to the power grids in the Persian Gulf area that it can be validated in a large scale of power system. Through the simulations of the single machine model and the multi-machines model that are interconnected with other neighboring power grids, it is examined the small signal stability in power system and verified the same trend of changing in damping ratio with theory by various operating conditions of generating units.

1.4. Dissertation Overview

This thesis is organized in following order to reflect the research objectives efficiently. The small signal stability on the aspect of the power system is presented in Chapter 2. The operating conditions of a generator by reactive capability curve are discussed in Chapter 3. The effect of operating condition of a generator on synchronizing and damping torque coefficient and damping ratio is expressed as a mathematical formula in Chapter 4. Chapter 5 presents case studies for the SMIB and a real-world power network model in order to support the theory about the effect on damping by operating conditions of generators. Finally, Chapter 6 summarizes and concludes the major point of this dissertation.

A brief description of each individual chapter is given as follows:

Chapter 1: This chapter briefly introduces the motive of this study and the background of stability in power system. The damping torque coefficient is expressed as a function of operating condition, and operating condition is determined by the range along the reactive capability curve by contrast with previous studies.

Chapter 2: From the dynamics of a synchronous machine, it is introduced how to evaluate damping ratio. The equations describing the dynamics of power system are non-linear, therefore it is linearized for the analysis of small signal stability. Next, it is expressed as a ‘state-space’ representation to determine the eigenvalues.

Chapter 3: The reactive capability curve is introduced in this chapter. It explains the thermal limits of a generator. For the understanding of reactive capability curve, initially, power angle and power factor are introduced. Accordingly, the physical (heating) limits of reactive capability curve in order to assure the safety of a synchronous machine are explained. It is also presented the permissible operating points along the curve and different operating conditions such as leading, unity and lagging.

Chapter 4: It is explained about two coefficients, synchronizing torque coefficient (K_S) and damping torque coefficient (K_D) that impact on damping in power system. They are expressed in terms of real and reactive power as mathematical formulae. It is examined the effect of operating conditions on these two coefficients and damping ratio as well.

Chapter 5: In this chapter, two different case studies are presented so as to validate the theoretical formulae on damping ratio in Chapter 4. First, it is demonstrated in a single machine environment, a SMIB model. Then, it has been expanded to the real-world power grids with four generating units and examined the trend of damping ratio by operating conditions of generators through the simulation.

Chapter 6: It is summarized the subject over entire thesis which is the effect on damping ratio by operating conditions of generators in this final chapter.

Chapter 2. Small Signal Stability

2.1. Power System Stability

Historically, it was not until 1920's that the power system stability started to get the industry's attention and be recognized as an important factor for secure system operation. The early stability problems were mainly associated with remote power plants that feed electric power to the load centers through transmission lines over long distances. [12] The major blackouts which happened in the Northeast in 2003, in the Southwest in 2011, in North America and the great blackout of September 2011 in Korea that brought chaos and a huge deal of economic loss imprinted the significance of power system stability. Evidently, it is significantly important to maintain phase angle, frequency, and voltage of power system constant and stable to avoid such disasters.

Power system stability is defined as the property of a power system that enables it to remain in a state of operating equilibrium under normal operating conditions and to regain an acceptable state of equilibrium after being subjected to a disturbance. [13] It can be classified as shown in Figure 2.1 based on the physical nature of the resulting mode of instability, the size of disturbances, the device, the process, the time span, and so forth. It is broadly divided into three major stabilities such as rotor angle stability,

frequency stability, and voltage stability according to the physical nature of system dynamics behavior.

Rotor angle stability is the ability of synchronous machines of an interconnected power systems to remain in synchronism after being subjected to disturbances. The rotor angle of a generator depends on the balance between the electromagnetic torque due to the generator electrical power output and mechanical torque due to the input mechanical power through a prime mover. [3]

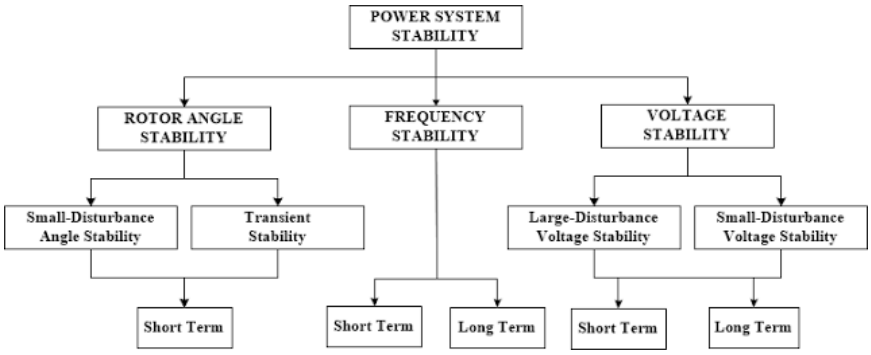

Figure 2.1 Classification of power system stability

Small-disturbance angle stability (or small signal stability), in particular, is the ability to maintain the synchronism without persisting the oscillation under the small disturbances. These disturbances occur continually on the system due to small variations in loads and generation. Therefore, it is essential to analyze small signal stability to scrutinize the effect of small disturbances on power system, thereby it is necessary to have a clear understanding on the dynamics of synchronous machine most of all.

2.2. Dynamics of Synchronous Machine

A simple power network model can be represented with a classical model of a generator which is composed of a constant voltage source ($\tilde{E}'$) behind the transient reactance (X'_d), an infinite bus ($\tilde{V}_s$), and the total reactance (X_T) connect them as shown in Figure 2.2. Here, all resistances are neglected.

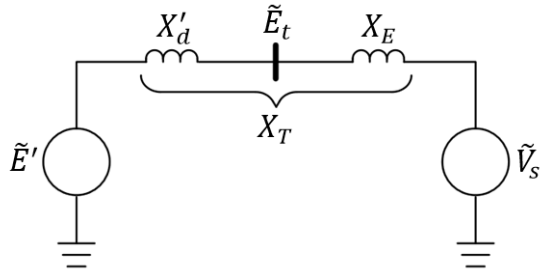

$$where \begin{cases} \tilde{E}' = transient\ \ emf\ \ of\ \ a\ \ generator \\ \tilde{E}_t = terminal\ \ voltage \\ \tilde{V}_s = infinite\ \ bus\ \ voltage \\ X_E = transfer\ \ reactance \\ X_T = total\ \ reactance \end{cases}$$

Figure 2.2 Simple power network model

The rotor of a synchronous generator is driven by a prime mover, and its dynamics presenting the effect of unbalance between the mechanical and electromagnetic torque which can be express as a 'Swing Equation' that signifies the swings in rotor angle (δ) during disturbance. The swing equation includes a component of damping torque as shown in Equation 2.1. Herein, the damping torque coefficient, K_D takes an important role in capturing power system transient behaviors. It will be explained in detail

later on together with synchronizing torque coefficient (K_S) in section 2.4.

$$\frac{2H}{\omega_0}\frac{d^2\delta}{dt^2} = T_m - T_e - K_D\Delta\omega_r \tag{2.1}$$

$$where \begin{cases} H = inertia \\ \omega_0 = rated\ \ angular\ \ velocity \\ \delta = power\ \ angle \\ T_m = mechanical\ \ torque\ \ [N \cdot m] \\ T_e = electromagnetic\ \ torque\ \ [N \cdot m] \\ K_D = damping\ \ torque\ \ coefficinet \\ \omega_r = rotor\ \ angular\ \ speed \end{cases}$$

In order to analyze the power system dynamic performance, it is required to express the component models as two first-order differential equations as shown in Equation 2.2 and 2.3 respectively, and they are often called as 'Equations of motion'.

$$\frac{d}{dt}\Delta\omega_r = \frac{1}{2H}(T_m - T_e - K_D\Delta\omega_r) \tag{2.2}$$

$$\frac{d}{dt}\delta = \omega_0\Delta\omega_r \tag{2.3}$$

$$where \begin{cases} \Delta\omega_r = per\ \ unit\ \ speed\ \ deviation \\ \delta = rotor\ \ angle \\ \omega_0 = base\ \ rotor\ \ electrical\ \ speed\ \ [rad/s] \end{cases}$$

2.3. Linearization of a Dynamic System

The dynamics of power system and its characteristic of equivalent equations describing it is non-linear. Hence, for the purpose of small signal analysis of power system, the non-linear differential and algebraic equation such as a swing equation should be linearized about a selected steady-state operating condition. Since the small disturbances are considered to be sufficiently small and the perturbations are assumed to be small, these make it possible that the nonlinear functions can be expressed in terms of a first-order Taylor's series expansion, by doing so it can be obtained the linearized forms of equations from them, and the linearization of system equations is suitable for the purposes of small-signal stability studies. In this technique, the characteristic of power system can be determined through a specific operating point and the stability of the system is clearly examined by the system eigenvalues. [9]

By linearizing Equation 2.2 and 2.3 and substituting for $\Delta T_e \ \ with \ \ K_S \Delta\delta$, the linearized equations can be transformed as Equation 2.4 and 2.5 respectively.

$$\frac{d}{dt}\Delta\omega_r = \frac{1}{2H}(\Delta T_m - K_S\Delta\delta - K_D\Delta\omega_r) \tag{2.4}$$

$$\frac{d}{dt}\delta = \omega_0\Delta\omega_r \tag{2.5}$$

$$where \begin{cases} \Delta\omega_r = per \ \ unit \ \ speed \ \ deviation \\ K_S = synchtonizing \ \ torque \ \ coefficient \\ K_D = damping \ \ torque \ \ coefficient \\ \delta = rotor \ \ angle \ \ [electrical \ \ radians] \\ \omega_0 = base \ \ rotor \ \ electrical \ \ speed \ \ [rad/s] \end{cases}$$

2.4. Synchronizing and Damping Torque Coefficient

In Equation 2.4, K_S is a synchronizing torque coefficient and K_D is a damping torque coefficient, and both of them are used to analyze the rotor angle stability. The synchronizing and damping torque coefficients should be positive for the stable operation of power system.

In electric power system, the change in electrical torque of a synchronous machine following a perturbation could be resolved into two components: $K_S\Delta\delta$ is the synchronizing torque component, which is the component of torque change in phase with the rotor angle perturbation ($\Delta\delta$), and $K_D\Delta\omega$ is the damping torque component, which is the component of torque in phase with the speed deviation ($\Delta\omega$). System stability depends on both components for the torque of a synchronous machine. [4]

$$\Delta T_e = \underbrace{K_S\Delta\delta}_{\substack{\text{synchronizing torque} \\ \text{component}}} + \underbrace{K_D\Delta\omega}_{\substack{\text{damping torque} \\ \text{component}}} \tag{2.6}$$

$$where \begin{cases} K_S: synchronizing\ \ torque\ \ coefficient \\ K_D: damping\ \ torque\ \ coefficient \\ \Delta\delta: rotor\ \ angle\ \ perturbation \\ \Delta\omega: angular\ \ speed\ \ deviation \end{cases}$$

The synchronizing torque is responsible for restoring the rotor angle deviations ($\Delta\delta$) and the damping torque damps out the speed deviations ($\Delta\omega$). The synchronizing and damping torques may be expressed in terms of synchronizing torque coefficient (K_S) and Damping torque coefficient (K_D) respectively as shown in Equation 2.6. These coefficients are often calculated for the purpose of assessment and evaluation of the

damping ratio since the damping ratio is dependent on these two coefficients. [10, 14]

2.5. State-Space Equation of System Equation

The classical control theory based on a simple input-output description is usually expressed as a transfer function. It does not utilize any information of the interior structure of the system, and it is quite limited in its applications. On the contrary, one of the modern control theory – 'state-space' representation, a mathematical model of a physical system as a set of input, output and state variables related by first-order differential equations provides a complete description of the dynamic system behavior along with the inputs to the systems. The state-space representation, therefore, is suited for the analysis of multi-variable multi-input and multi-output systems.

The general formulation for the state-space representation of a linear system is a set of coupled, first-order differential equation as shown in Equation 2.7.

$$\dot{x} = \mathrm{Ax} + \mathrm{Bu} \tag{2.7}$$

$$where \begin{cases} A = state\ \ matrix \\ x = the\ \ vector\ \ of\ \ state\ \ variables \\ B = the\ \ input\ \ matrix \\ u = the\ \ vector\ \ of\ \ control\ \ inputs \end{cases}$$

From Equation 2.7, it can be obtained a system equation as a state-space representation has a vector-matrix form like Equation 2.8.

$$\begin{bmatrix} \Delta\dot{\omega}_r \\ \Delta\dot{\delta} \end{bmatrix} = \begin{bmatrix} -\frac{K_D}{2H} & -\frac{K_S}{2H} \\ \omega_0 & 0 \end{bmatrix} \begin{bmatrix} \Delta\omega_r \\ \Delta\delta \end{bmatrix} + \begin{bmatrix} -\frac{1}{2H} \\ 0 \end{bmatrix} \Delta T_m \tag{2.8}$$

Here, the state matrix A (or A matrix) is a following two by two square matrix as shown in Equation 2.9.

$$A = \begin{bmatrix} -\frac{K_D}{2H} & -\frac{K_S}{2H} \\ \omega_0 & 0 \end{bmatrix} \tag{2.9}$$

The second-order characteristic equation can be expressed as Equation 2.10 by means of a damping torque coefficient (K_D) and a synchronizing torque coefficient (K_S).

$$s^2 + \frac{K_D}{2H}s + \frac{K_S\omega_0}{2H} = 0 \tag{2.10}$$

It can also be written as a general form like Equation 2.11 in terms of undamped natural frequency (ω_n) and damping ratio (ζ).

$$s^2 + 2\zeta\omega_n s + \omega_n^2 = 0 \tag{2.11}$$

$$where \begin{cases} \omega_n = undamped \quad natural \ \ frequency \\ \zeta = damping \ \ ratio \end{cases}$$

2.6. Eigenvalues and Damping Ratio

The two sets of roots are easily found using the quadratic formula in solving for the general form of equation in Equation 2.11 as shown in Equation 2.12.

$$\lambda_{1,2} = -\zeta\omega_n \pm j\omega_n\sqrt{\zeta^2 - 1} \tag{2.12}$$

A conjugate pair of complex eigenvalues which is associated with oscillatory modes of response can be presented as Equation 2.13.

$$\lambda = \sigma \pm j\omega \tag{2.13}$$

$$where \begin{cases} \sigma = \ -\zeta\omega_n = \dfrac{K_D}{4H} \\ \omega = \omega_n\sqrt{\zeta^2 - 1} \end{cases}$$

Here, σ, the real part of complex eigenvalue is a decrement factor depicted as the growth or decay rate of an exponential envelope around the oscillations, and it indicates the damping of the oscillation (or attenuation). Meanwhile, ω, the imaginary part of a complex eigenvalue is a damped natural frequency [rad/s] or an eigenfrequency that determines the observed frequency of the oscillations. The complex eigenvalue with a negative real part gives an exponentially decaying magnitude of the mode (asymptotically stable), and that with a positive real part signifies the oscillations with a growing magnitude with time, i.e. an unstable oscillatory mode. [15]

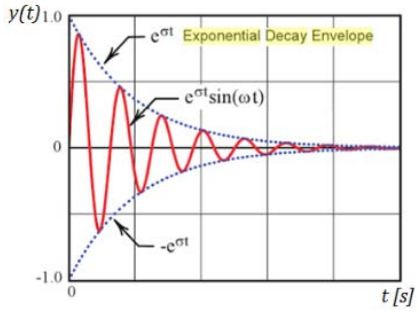

Figure 2.3 Decaying oscillations

The damping of the oscillations can be evaluated by means of the damping ratio (ζ) as shown in Equation 2.14, and the range for damping ratio of a decaying oscillatory mode is limited from zero to one, i.e. $0 < \zeta < 1$.

$$\zeta = -\frac{\sigma}{\omega_n} = \frac{-\sigma}{\sqrt{\sigma^2+\omega^2}} \tag{2.14}$$

Meanwhile, the damping ratio also can be expressed in terms of a damping torque coefficient (K_D) and a synchronizing torque coefficient (K_S). From the relationship between the characteristic equation - Equation 2.10 and the general form - Equation 2.11, the damping ratio can be presented as Equation 2.15.

$$\zeta = \frac{1}{2}\frac{K_D}{\sqrt{K_S 2H\omega_0}} \tag{2.15}$$

$$where \begin{cases} K_D = 4H\sigma = -4H\zeta\omega_n \\ K_S = \dfrac{2H\omega_n^2}{\omega_0} = \dfrac{EV}{X_T}\cos\delta \end{cases}$$

So far, it is examined the damping ratio considering the deviation of rotor angular speed and that of rotor angle (power angle) only. However, in practice it should be considered many other state variables such as the effect of field flux linkage variations ($\Delta\psi_{fd}$), excitation system, power

system stabilizer (PSS), amortisseurs, and so forth in order to evaluate the system performance and the damping ratio for the real-world power system precisely.

As the state variables are expanded, the system equation as a state-space representation in Equation 2.8 will grow in its dimension, and the state-matrix in Equation 2.9 can be expressed as a form of general n x n square matrix as shown in Equation 2.16. The state matrix is equivalent to the Jacobian matrix evaluated at the equilibrium point, and it is referred to as the 'A matrix' or the 'plant matrix' as well.

$$\mathrm{A} = \begin{bmatrix} \frac{\partial f_1}{\partial x_1} & \cdots & \frac{\partial f_1}{\partial x_n} \\ \cdots & \ddots & \cdots \\ \frac{\partial f_n}{\partial x_1} & \cdots & \frac{\partial f_n}{\partial x_n} \end{bmatrix} \tag{2.16}$$

For a given power system, in general, the stability can be assessed by evaluating the eigenvalues of a state matrix (A matrix) according to the linear control theory.

$$|\lambda I - A| = 0 \tag{2.17}$$

$$where \begin{cases} \lambda = vector\ \ of\ \ eigenvalues \\ I = identity\ \ matrix \\ A = state\ \ matrix \end{cases}$$

Eigenvalues for a given state matrix (A matrix) can be calculated by solving above Equation 2.17. Likewise, a conjugate pair of complex eigenvalues can be expressed as Equation 2.13, and the damping ratio can be evaluated with the formula as shown in Equation 2.14 respectively.

Chapter 3. Operating Condition of Generators

3.1. Power of a Generator

In general, generating capacity in power system is referred to as the “real power output (P)”. This indicates the ability on how much power is generated by a generator. It is measured and represented as a unit of KW or MW. The mechanical output of the prime mover controls the generation. With this, if losses are considered insignificant, the electrical power output from the turbine is equivalent to that of a generator.

Nevertheless, the appropriate measure of the capacity of the synchronous generator is the apparent power (|S|) which is the magnitude of complex power. It could be calculated by the mathematical formula, $|S| = \sqrt{P^2 + Q^2}$, and is expressed in a unit of KVA or MVA as shown in Figure 3.1. Real power (P) is simply the power that does actual work, while reactive power (Q) is the power required to establish and maintain magnetic field that oscillates between source and load, and it is independent of the prime mover.

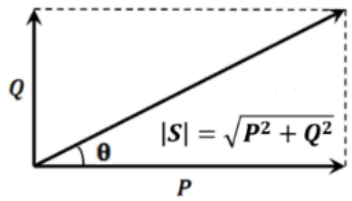

Figure 3.1 Real, reactive, and apparent power

3.2. Power Angle and Power Factor

Power factor (represented as PE) is the measure of the efficiency of a generator in producing real power, P [KW] with respect to apparent power $|S|$ [KVA], the total amount of power 'being applied' as shown in Equation 3.1. In general, the power factor of a generator could be quantified as 1 or less than 1, i.e. PF≤1, in Equation 3.1. This is because power angle (θ) can only range between -90° (or $-\frac{\pi}{2}$) and +90° (or $+\frac{\pi}{2}$), and the values of cosine functions in the first and fourth quadrants are always positive. Accordingly, the power factor represented as $cos(\theta)$ is always positive unquestionably. Hence, the only way to determine whether the power angle is negative, 1, or positive from the power factor is to denote it as leading, unity or lagging.

$$Power\ \ factor = cos(\theta) = \frac{P}{|S|} \tag{3.1}$$

$$where \begin{cases} \theta = \ power\ \ angle \\ P = real\ \ power \\ |S| = apparent\ \ power \end{cases}$$

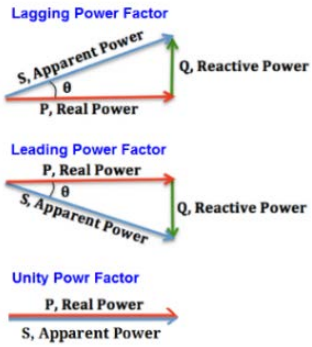

Figure 3.2 Power factor as a generator context

Unity power factor, i.e. PF=1, which is the maximum value of power factor, signifies that the generator is 100% efficient at producing real power P [KW], accordingly the leading or lagging power factor should always be less than 1. In the context of the power generation in a synchronous generator, lagging power factor means that the generator injects (produces) reactive power Q [VAR] at over-excited regime, with respect to the maximum value of reactive power (Q_{max}) defined by the capability curve i.e. $S = P + jQ$. On the other hand, leading power factor, the generator absorbs (consumes) reactive power Q [VAR] at under-excited regime, with respect to the minimum value of reactive power (Q_{min}) described by the capability curve i.e. $S = P - jQ$ as shown in Figure 3.2.

3.3. Reactive Capability Curve

In an operating context, it is vital to determine and maintain a generator's operation within its safe extent and condition without overheating or malfunctioning due to high current. Overheating can result in an internal fault or short circuit. This could lead to the deterioration of insulating material in the generator windings. Therefore, a generator should be operated within the limits that can assure the safety of the machine. Generally, these limits are indicated by the generator rating in KVA or MVA. [16]

It is significantly important to consider the reactive capability limit of a synchronous generator in that the range of safe operation for a generator regarding stability studies. The boundary on permissible combinations of real and reactive power output is called "reactive capability curve" which expresses the capability and limitation of a generator significantly. Different parts of the capability curve are limited by different mechanical components. The capability of real and reactive power output is restricted by the following major constructional and operational constraints as shown in Figure 3.3:

1) **Armature (stator) current limit** – the heating limit on the power output imposed by the stator copper power loss (I^2R) due to armature current (described as a circular arc $\widehat{BF}$ in the P-Q plane).

In the P-Q plane, the armature current corresponds to a circle represented as the equation of a circle, $P^2 + Q^2 = (VI_{max})^2$

2) **Field (rotor) current limit** – the limit to the field current of a generator imposed by copper power loss ($I_{fd}^2 R_{fd}$) in the rotor winding (drawn as a circular arc $\widehat{AB}$ in the P-Q plane). In the P-Q plane, the rotor current corresponds to a circle expressed as the mathematical formula of a circle, $P^2 + (Q + V^2/x_d)^2 = (E_{q.max}V/x_d)^2$.

3) **Stator-end region heating limit** – the limit to the generator in the under-excited region by the localized heating in the end region of stator results from eddy currents in the laminations due to the end-turn leakage flux (depicted as a line segment $\overline{FG}$ in the P-Q plane). There's no simple mathematical formula describing this constraint, the relevant curve has to be determined experimentally by the manufacturer.

4) **The power angle limit** – the limit concerning the maximum value of the power angle (δ) (expressed as a line segment $\overline{GH}$ in the P-Q plane). In the P-Q plane, the limit can be expressed as a straight line in the formula of $P = \tan(\delta_{MAX})\, Q + (V^2/x_d)\tan(\delta_{MAX})$.

5) **The real power limit** – the limit is concerned with turbine power and depends on the type of turbine. The upper constraint P_{max} is due to the maximum (rated) output of the turbine (drawn as a vertical line segment $\overline{CE}$ in the P-Q plane), while the lower

constraint P_{min} is due to the stable operation of boilers (burners) at a low turbine output (drawn as a vertical line segment $\overline{AH}$ in the P-Q plane).

This curve shows not only the relationship of real, reactive, and apparent power, but also generator limitations at different operating conditions. The operating points are established based on current PF, real power P [MW], and temperature. [4, 17]

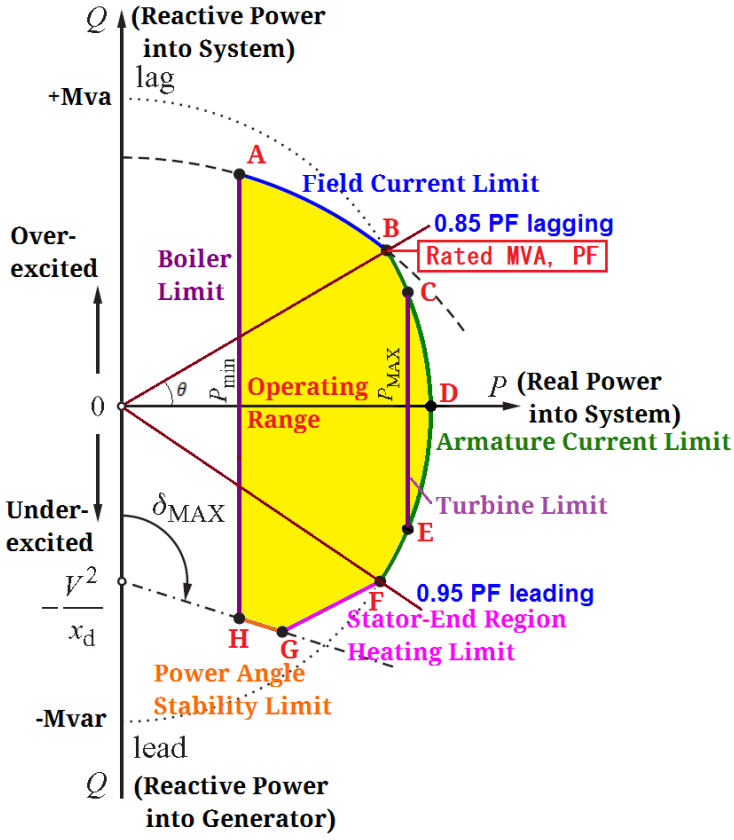

Figure 3.3 Reactive capability curve of a synchronous generator

3.4. Power Factor and Operating Points

The power factor is an important factor that must be considered for the safe operation of a generator. The point B, where the circles of filed current limit and armature-current limit intersect each other in the P-Q plane, represents the machine nameplate MVA and power factor rating, which is 0.85 lagging power factor in Figure 3.3. The synchronous generators are rated in terms of the maximum reactive [MVA] output at the specified voltage and power factor, normally 0.8, 0.85, or 0.9 lagging, that they can carry continuously without overheating and operate under steady state condition. [18]

All the points within the border lines bounded by constraints illustrated as the polygon ABCDEFGH are achievable without any risk of damages, considering the criteria of safe operating points in a generator, whereas that outside curves are prohibited. Operation outside of this area can have adverse effects such as overheating on generator performance and may result to damage. The typical operating range of a synchronous generator is usually between the lagging power factor of 0.85 and the leading power factor of 0.95 as indicated in Figure 3.3, and it should not to exceed this limit. The applicable segments of the reactive capability curve are the points between the point B and F in Figure 3.3. [16] Furthermore, “Synchronous Generating Units, when supplying Rated MW, are required to be able to operate continuously at any power factor between 0.95 power

factor leading and 0.85 power factor lagging at the Generating Unit terminals in accordance with CC.6.3.2 of the Grid Code". [19]

It is concluded that the operating condition of a generator will be indicated as 'lagging', 'leading' or 'unity' of power factor respectively according to the location of operating points within the boundary of the reactive capability curve. This determines the operational mode of the generation in plants. In order to assure the safe operation of a generator, the operating points, therefore, should not exceed the normal operating range typically between power factor of 0.85 lagging and 0.95 leading that is determined by the specification of a generator from manufacturers. If the effect of turbine is ignored, the operating points of a synchronous generator that can generate maximum power output will be the points along the circular segments from the point B to F, i.e. $\widehat{BF}$. That is, the maximum range of operating points of a generator will be lied on the reactive capability curve, from the point F for leading, via the point D for unity, to the point B for lagging in Figure 3.3. These three operating points of a generator will be used later on for the operating conditions in the simulations in Chapter 5.

Chapter 4. Effect on Damping by Operating Conditions

4.1. Emf of Generator and Infinite Bus Voltage

The simple power network with a synchronous generator is connected to an infinite bus, through a total impedance (X_T), and if all resistances (R) are neglected, the system representation can be depicted schematically as shown in Figure 4.1. Herein, X_T represents the total reactance between two nodes, $\tilde{E}'$ and $\tilde{V}_s$. It is the sum of the direct axis transient reactance (X'_d) and transfer reactance (X_E) that is $X_T = X'_d + X_E$. The transfer reactance (X_E) is the combination of the step-up transformer (X_{TR}) and that of the equivalent network (X_L), that is $X_E = X_{TR} + X_L$.

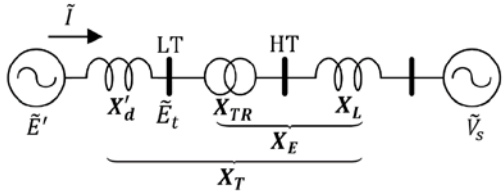

Figure 4.1 Simple network system representation

In Figure 4.1, the transient electromotive force (emf) of a generator ($\tilde{E}'$) is the voltage behind transient reactance (X'_d), and $\tilde{V}_s$ is the voltage of an infinite bus and it can be evaluated by deriving the equation from the formula for complex power. The complex power can be defined as the product of voltage phasor ($\tilde{E}'$) and conjugate of current phasor ($\tilde{I}^*$) as shown in Equation 4.1. In power system analysis, complex power ($\tilde{S}$) is

also often represented as a combination of real power (P) and reactive power (Q) in a form of $\tilde{S} = P + jQ$ and it is represented as Equation 4.1.

$$\tilde{S} \equiv \tilde{E}' \cdot \tilde{I}^* = P + jQ \tag{4.1}$$

The current ($\tilde{I}$) flows along the power system can be derived from the above equation into the following equation.

$$\tilde{I} = \frac{P - jQ}{\tilde{E}'^*} \tag{4.2}$$

The transient emf of a generator ($\tilde{E}'$) can be expressed as Equation 4.3 by expressing the simple network system in Figure 4.1.

$$\tilde{E}' = jX_T \cdot \tilde{I} + \tilde{V}_s \tag{4.3}$$

By substituting the current ($\tilde{I}$) in Equation 4.2 for that in Equation 4.3, then the emf of a generator, $\tilde{E}'$ can be re-written as Equation 4.4.

$$\tilde{E}' = jX_T \cdot \left(\frac{P - jQ}{\tilde{E}'^*}\right) + \tilde{V}_s \tag{4.4}$$

Therefore, the infinite bus voltage ($\tilde{V}_s$) can be represented like Equation 4.5 in terms of real power (P) and reactive power (Q). This infinite bus voltage ($\tilde{V}_s$) is essential to evaluate a synchronizing torque coefficient (K_S) and a damping torque coefficient (K_D) in the following section 4.2.

$$\tilde{V}_s = \tilde{E}' - jX_T \cdot \left(\frac{P - jQ}{\tilde{E}'^*}\right) \tag{4.5}$$

4.2. Synchronizing and Damping Torque Coefficient

Recall that the damping ratio (ζ) can be expressed in terms of two coefficients that are the synchronizing torque coefficient (K_S) and the damping torque coefficient (K_D). In connection with this, damping ratio is directly proportional to the damping torque coefficient and inversely proportional to the square root of synchronizing torque coefficient as shown in Equation 4.6. Since H is an inertia constant and ω_0 is the rated angular speed in electrical radian, given as $\omega_0 = 2\pi f_0$, it is obvious that the only variables that effect on damping are synchronizing torque coefficient (K_S) and damping torque coefficient (K_D).

$$\zeta = \frac{1}{2}\frac{K_D}{\sqrt{K_S 2H\omega_0}} \tag{4.6}$$

As it is already examined in Chapter 3, the operating conditions such as ‘leading’, ’unity’ and ‘lagging’ are determined by power factors with components of real power (P) and reactive power (Q). Subsequently, it is crucial to find out the correlation between each operating condition and damping torque coefficient and synchronizing torque coefficient respectively in order to analyze the effect on damping by operating conditions.

Evidently, it is very simple to figure out the relationship between power factor and synchronizing torque coefficient (K_S). As it is defined in

Chapter 3, real power (P) and reactive power (Q) are defined as Equations 4.7 and 4.8.

$$P = \frac{|\tilde{E}'||\tilde{V}_s|}{X_T}\sin\delta \tag{4.7}$$

$$Q = \frac{|\tilde{E}'|^2 - |\tilde{E}'||\tilde{V}_s|}{X_T}\cos\delta \tag{4.8}$$

$$where\ \ \delta = \theta_{\tilde{E}'} - \theta_{\tilde{V}_s}$$

Supposing that a synchronous generator is a round-rotor typed machine, then by letting combined direct axis reactance (x'_d) and combined quadrature axis (x'_q) are the same as the total reactance (X_T), that is $x'_d = x'_q = X_T$, where $x'_d = X'_d + X_E$ and $x'_q = X'_q + X_E$, it can be established a relationship between power factor and synchronizing torque coefficient (K_S) by differentiating the real power (P) as shown in Equation 4.9.

$$K_s \equiv \frac{dP_e}{d\delta} = \frac{|\tilde{E}'||\tilde{V}_s|}{X_T}cos\,\delta = \frac{|\tilde{E}'||\tilde{V}_s|}{X_T}cos(\theta_{\tilde{E}'} - \theta_{\tilde{V}_s}) \tag{4.9}$$

$$where\ \begin{cases} \tilde{E}' = transient\ \ emf\ \ of\ \ a\ \ generator \\ \tilde{V}_s = infinite\ \ bus\ \ voltage \\ X_T = total\ \ reactance\ \ between\ \ two\ \ nodes \\ \delta = \ \theta_{\tilde{E}'} - \theta_{\tilde{V}_s} \end{cases}$$

By substituting $\left|\tilde{V}_s\right|$ in Equation 4.9 with that in Equation 4.5, the synchronizing torque coefficient can be re-written as Equation 4.10.

$$K_S = \frac{|\tilde{E}'|\cdot\left|\tilde{E}' - jX_T\cdot\left(\frac{P-jQ}{\tilde{E}'^*}\right)\right|}{X_T}\cos(\theta_{\tilde{E}'} - \theta_{\tilde{V}_s}) \tag{4.10}$$

On the other hand, damping torque coefficient (K_D) can be defined as the product of damping torque constant (D_d) and the square of the

magnitude of infinite bus voltage ($\left|\tilde{V}_s\right|^2$) as shown in Equation 4.11, and the damping torque constant (D_d) can be expressed as Equation 4.12 respectively. [17]

$$K_D \equiv D_d \cdot \left|\tilde{V}_s\right|^2 \tag{4.11}$$

$$where\ \ D_d = damping\ \ torque\ \ constant$$

$$D_d = \left(\frac{X'_d - X''_d}{(X'_d + X_E)^2}\frac{X'_d}{X''_d}T''_d \sin^2\delta + \frac{X'_q - X''_q}{(X'_q + X_E)^2}\frac{X'_q}{X''_q}T''_q \cos^2\delta\right)\omega_0 \tag{4.12}$$

$$where \begin{cases} X'_d = direct\ \ axis\ \ transient\ \ reactance \\ X''_d = direct\ \ axis\ \ sub-transient\ \ reactance \\ X'_q = quadrature\ \ axis\ \ transient\ \ reactance \\ X''_q = quadrature\ \ axis\ \ sub-transient\ \ reactance \\ X_E = transfer\ \ reactance\ \ between\ \ two\ \ nodes = X_{TR} + X_L \\ T''_d = d-axis\ \ short-circuit\ \ sub-transient\ \ time\ \ constant \\ T''_q = q-axis\ \ short-circuit\ \ sub-transient\ \ time\ \ constant \\ \delta = \theta_{\tilde{E}'} - \theta_{\tilde{V}_s} \\ \omega_0 = the\ \ rated\ \ angular\ \ speed\ \ in\ \ electrical\ \ radian\ \ = 2\pi f_0 \end{cases}$$

Herein, it will be revolved around a round-rotor typed generator for the purpose of simplification. For a round-rotor typed synchronous machine, suppose that combined direct axis reactance (x'_d) and combined quadrature axis (x'_q) are the same as the total reactance (X_T), that is $x'_d = x'_q = X_T$, then the above equation can be reduced into a following simple equation. [17]

$$D_d = \left(\frac{X'_d - X''_d}{(X'_d + X_E)^2}\frac{X'_d}{X''_d}T''_d\right)\omega_0 \tag{4.13}$$

Hence, in accordance with Equations 4.5 and 4.13, by plugging them into Equation 4.11, the damping torque coefficient (K_D) can be expressed in terms of the real and reactive power like Equation 4.14.

$$K_D = \left(\frac{X'_d - X''_d}{(X'_d + X_E)^2} \frac{X'_d}{X''_d} T''_d\right) \omega_0 \cdot \left|\tilde{E}' - jX_T \cdot \left(\frac{P - jQ}{\tilde{E}'^*}\right)\right|^2 \quad (4.14)$$

4.3. Effect of Operating condition

Note that it is difficult to estimate the impact of real and reactive power on synchronizing torque coefficient (K_S) and damping torque coefficient (K_D) with equations in section 4.2 intuitionally. For the simplification of these equations, it is desirable to separate the variables from other terms. In the equations for K_S and K_D in Equation 4.10 and 4.14, the real power (P) and reactive power (Q) are the variables, and so does the angle difference between generator bus voltage and bus voltage, i.e. $\theta_{\tilde{E}'} - \theta_{\tilde{V}_s}$. On the other hand, the transient emf of a generator, $\tilde{E}'$ is fixed as 1 [pu] in its magnitude and the phase angle as the reference angle set to 0 degree, i.e. $\tilde{E}' = 1\angle 0°$. It is clear that the total impedance X_T is a calculated parameter, all the rest of transient and sub-transient impedances are constants of a generator, T_d'' is a time constant of a generator, and the rated angular speed in electrical radian (ω_0) is also a constant that is given as $2\pi f_0$. As a result, the synchronizing torque coefficient (K_S) is a function of P, Q and $\theta_{\tilde{E}'} - \theta_{\tilde{V}_s}$, and the damping torque coefficient (K_D) is that of P and Q respectively.

The graph pertains to the impact on K_S and K_D of operating condition composed of real and reactive power components would be a good visual indicator for the intuitive and effective perception. In order to draw a graph, it is necessary to calculate the values of real and reactive power. For the given operating conditions, when the apparent power ($|S|$)

is given, the real and reactive power can be calculated by utilizing the equation of apparent power and that of power factor (PF) like Equation 4.15 and 4.16 respectively.

$$|S| = \sqrt{P^2 + Q^2} \tag{4.15}$$

$$PF = cos(\theta) = \frac{P}{|S|} \tag{4.16}$$

Simply, the real and reactive power can be evaluated by a simple mathematical transposition process as shown in Equation 4.17 and 4.18 respectively.

$$P = |S| \cdot PF \tag{4.17}$$

$$Q = \sqrt{|S|^2 - P^2} \tag{4.18}$$

Accordingly, the values of synchronizing torque coefficient (K_S) and damping torque coefficient (K_D) are computed by plugging that of real and reactive power into Equation 4.10 and 4.14. For the calculation of K_S and K_D, a round-rotor typed synchronous generator model (GENROU) was employed. The detailed parameters of this specific generator are listed in Appendix 1. Here, note that the effect of a governor, exciter, and PSS are not considered. The resultant values of each synchronizing and damping torque coefficient as a function of the input of real and reactive power were plotted on a line graph over operating conditions. Figure 4.2 shows the relationship of operating conditions vs. synchronizing torque coefficient (K_S) and damping torque coefficient (K_D).

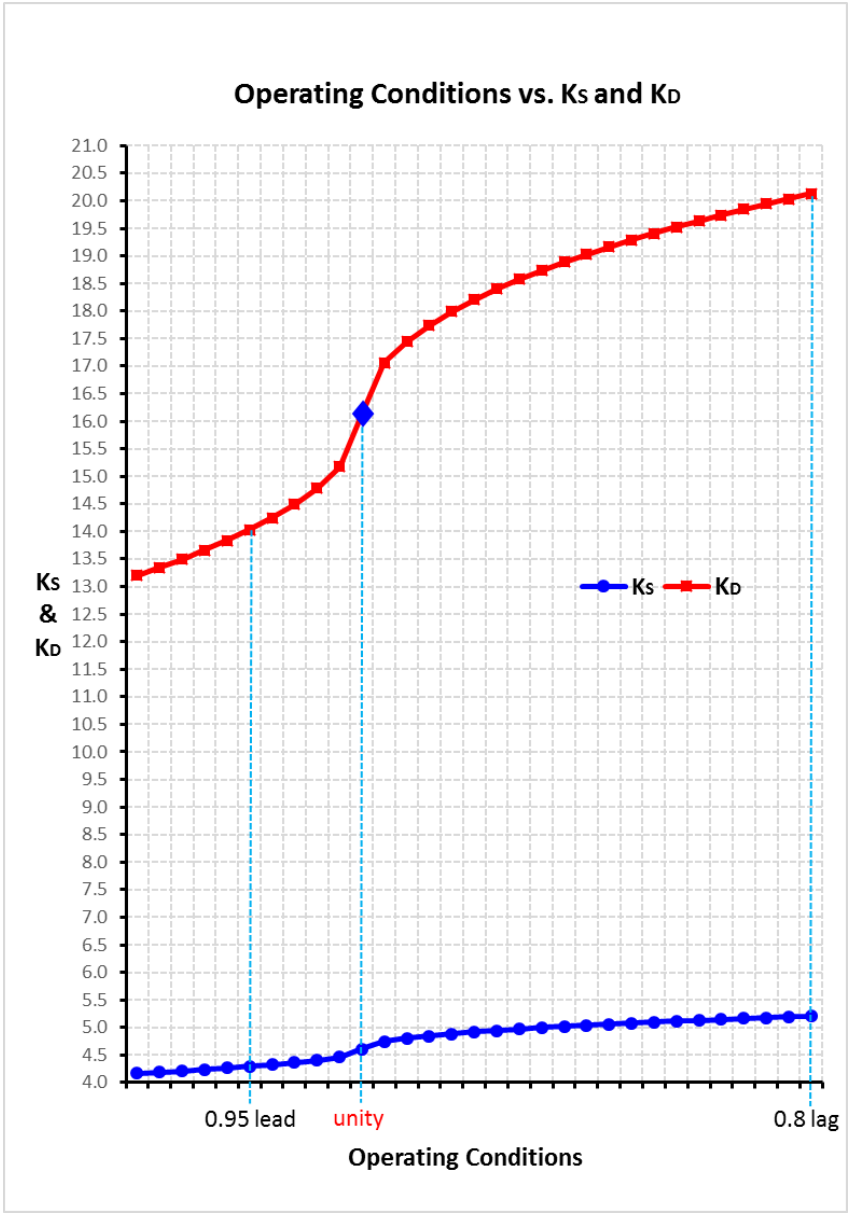

Figure 4.2 Graph on operating conditions vs. K_S and K_D

Clearly it can be analyzed, by intuition, that the values of synchronizing torque coefficient (K_S) increases as the operating condition changes from 0.95 leading via unity ($PF = 1$) to 0.8 lagging, likewise so does that of damping torque coefficient (K_D).

As mentioned earlier in this chapter, damping ratio (ζ) is directly proportional to a damping torque coefficient (K_D) and inversely proportional to the square root of synchronizing torque coefficient (K_S) like Equation 4.6. As a natural consequence of linear relationship between K_D and ζ, damping ratio increases as damping torque coefficient grows bigger. However, in case of synchronizing torque coefficient (K_S), a denominator in Equation 4.6, the damping ratio (ζ) increases even though it rises slightly.

As already discussed, in electric power system the change in electrical torque of synchronous machine following a perturbation is composed of both synchronizing and damping torque components. It manifests that the rate of increase in damping torque coefficient (K_D) is steep, while that in synchronizing torque coefficient (K_S) is gentle when the result was carefully scrutinized. That is, the value of damping torque coefficient increased sharply compared to that of synchronizing torque coefficient along the change of operating conditions from leading via unity to lagging. In other words, the damping torque coefficient impacts more heavily on damping ratio compared to synchronizing torque coefficient. Consequently, the damping ratio increases by the rise of both coefficients.

As a summary, the effect of change in operating conditions from leading via unity to lagging is to increase synchronizing torque coefficient slightly and increase damping torque coefficient considerably, subsequently such increases enhance the damping of rotor oscillations. This

trend could be confirmed through the graph on the relationship of operating conditions vs. damping ratio (ζ) as shown in Figure 4.3.

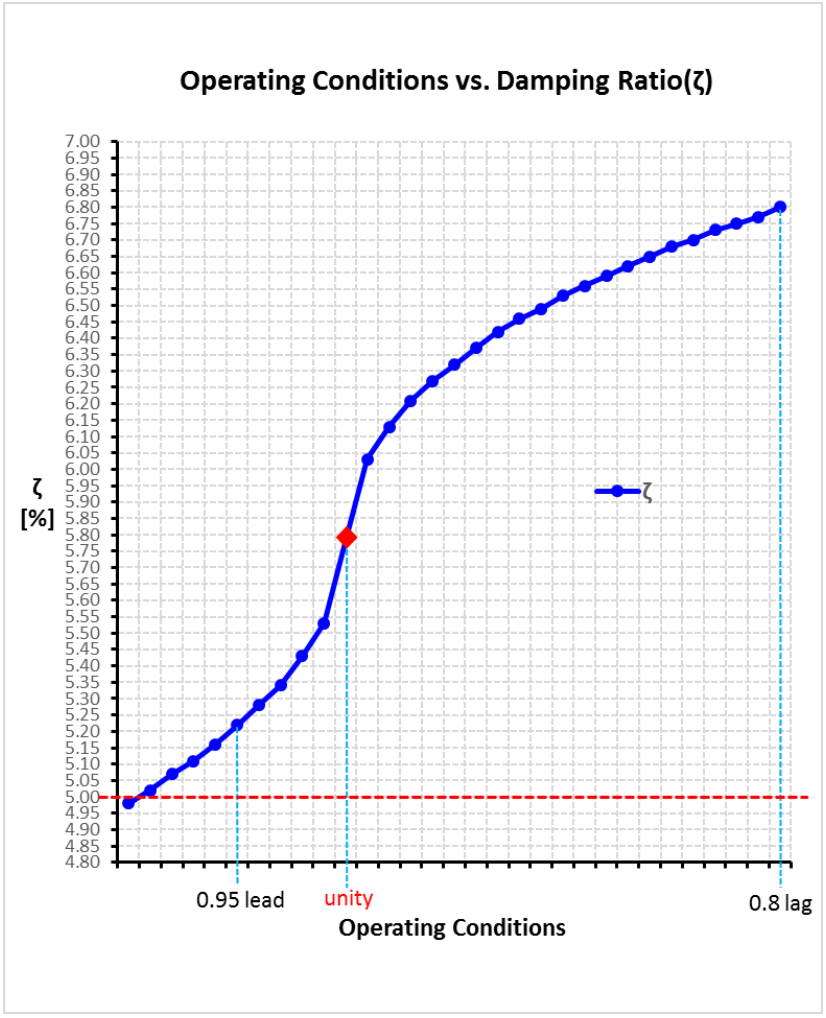

Figure 4.3 Graph on operating conditions vs. damping ratio (ζ)

As shown, the effect of operating conditions on damping ratio is demonstrated theoretically by the derived equations and plotted graphs. Such phenomena could be confirmed by conducting the simulations in Chapter 5 so that they can support the theory in this paper.

4.4. Damping Ratio and Stability

It is required to ensure the stability of power system following small disturbances. In order to maintain a secure system, it is necessary to make all generators run closely in synchronism. The most common measure for a stability analysis is the simulation in a time domain which is suitable for both large and small signal stability studies. On the other hand, modal analysis (or eigenvalue analysis) is exclusively suitable for the small signal stability in a frequency domain. Modal analysis is a good measure that describes the small signal behavior of a power system. It is typically used for the studies on inter-area oscillations, sub-synchronous torsional interactions, voltage stability, and so forth. [19] The behavior linearized around an operating point and the linear systems can be analyzed more efficiently than nonlinear systems by modal analysis, however it does not take the non-linear behavior of controllers into account. Hence, in order to analyze the stability of power systems more efficiently and systematically, not only the time domain analysis but also modal analysis (frequency domain analysis) should be measured and they have to be complemented each other.

In order to analyze the small signal stability, a powerful tool for modal analysis, NEVA was used in the simulations of this paper. NEVA provides with a good graphical index for the better understanding the result of a modal analysis. It focuses on investigations of dynamic behavior of a power system under different characteristic frequencies (aka. “modes”). In

a power system, all modes should be stable and all electromechanical oscillations should be damped out quickly. For this, all modes should be located on the left side of imaginary axis in a complex s-plane. The damping ratio will be plotted on a complex s-plane based on the eigenvalues. The axis of abscissas is the real part of complex eigenvalues which stands for the decrement factor (σ), and the axis of ordinates is the imaginary part of complex eigenvalues which signifies the damped natural frequency (ω). The damping ratio is the angle between the axis of ordinates (imaginary axis) and the 'isoline' from the eigenvalues to the origin and it is represented in percentage (%) as shown in Figure 4.4.

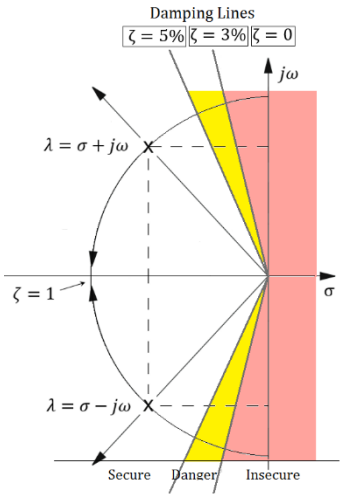

Figure 4.4 Damping ratio on a complex s-plane

The minimum acceptable level of damping is not clearly known. However, it is considered that a damping ratio of swing mode, the prime interest in studies of local and inter area oscillations in power systems, should be 5% or higher ($\zeta \geq 0.05$), that is it should be located on the left

side of 5% isoline in a complex s-plane, in order to ensure the stability of power system. A damping ratio is considered to be sufficient if it is 5% or above that is located in the secure zone in Figure 4.4. A damping ratio between 3% and 5% considered as weakly damped which is located in danger region and still acceptable. If a damping ratio is less than 3%, it is regarded as too weakly damped and located in insecure area which should be accepted with caution. Figure 4.5 shows the damping ratio on a second-order system. A damping ratio of 5% means that the amplitude is damped out to approximately 32% of its initial value in three oscillation periods (3T). [20]

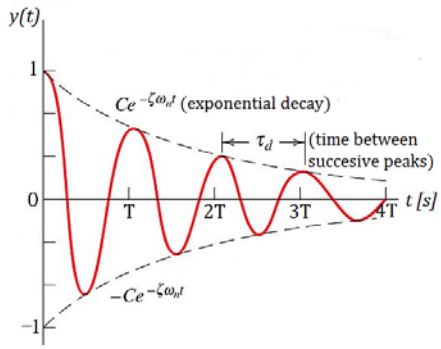

Figure 4.5 Damping ratio on a second order system

Therefore, the generators should be operated under the operating condition that satisfies the damping ratio with 5% or higher to ensure the stability of entire power system. For example, in Figure 4.3 the range of operating condition for a generator to assure the power system stability should be from 0.91 leading to 0.8 lagging of power factor which satisfies 5% or above in damping ratio (ζ).

Chapter 5. Case Study

5.1. Introduction

In this paper, two different scenarios are selected in order to validate the theory in Chapter 4 in relation to the effect on damping ratio by operating condition of a synchronous generator; The first scenario is the case of a single machine infinite bus system (SMIB) which is represented as a single generator is connected to an infinite bus through a transformer and a transmission line like Figure 4.1 in Chapter 4. Through this simulation on a simple power system, it will be validated that the expected change in damping ratio by different operating conditions in mathematical computation is match with the result from the simulation so as to make sure the theory is corroborated by the result of simulation. Then, the simulation will be expanded to the power system which is composed of multi-buses with four selected generating units. In the second scenario, the existing real-world power networks in the Persian Gulf are employed for the simulation. The power grids along the Persian Gulf are composed of numerous generating units that are interconnected to one another, and are setting up of couple new generators. [21]

In this case study, it will be verified that the damping is enough in each generating unit to damp out the oscillation of power system, as well as the damping ratio enhances as operating condition of generators change from leading via unity to lagging as expected in mathematical computation

in Chapter 4. Through this verification, it can be ensured that the newly added generating units would not adversely affect the existing ambient power plants and the stability is secured over the entire power grids along the Persian Gulf.

In order to perform simulations in this case study, a power system simulation software PSS/E (Power System Simulator for Engineering) and its modular component NEVA (Netomac EigenValue Analysis) for small signal analysis are employed. PSS/E is a robust software for electrical transmission networks that can simulate and analyze power system performance by Siemens. It is a comprehensive set of analysis programs designed to analyze the performance of power system both in steady-state and dynamic conditions. It has a variety of analysis functions with a graphical user interface such as power flow, OPF (Optical Power Flow), dynamic simulation, fault analysis and so on. The database 'Network Data' includes all the characteristics of power system such as bus, branch, machine, load, fixed shunt and switched shunt. The plot is drawn as an one-line diagram with essential information on a screen. A load flow simulation can be run by solving the load flow solutions. It provides several different solution methods such as 'Fixed Slope Decoupled Newton-Rapson', 'Full Newton-Rapson', and 'Decoupled Newton-Rapson'. A dynamics simulation will be run by calling a 'dynamics file', and by running the menu 'launching NEVA eigenvalue analysis', it will perform the modal analysis to calculate eigenvalues. It also extends the PSS/E dynamics analysis

capability to allow detailed investigation of small signal oscillations as well as indicating the optimum location and testing of corrective devices. [20] NEVA is a robust tool that provides with a visual index of small signal stability through the plot of the modes on a complex s-plane. It will evaluate eigenvalues (λ) and display many information such as decrement factor (σ), damped natural frequency (ω), eigenvectors, damping ratio (ζ), bode plot and so forth graphically so as to recognized them easily by intuition.

5.2. SMIB Model

In the first scenario, the simple power network which is referred as SMIB model is modeled with a synchronous generator and an infinite bus, and they are connected with a two-winding transformer and a transmission line. This model was created as one-line diagram representation using PSS/E software as shown in Figure 5.1.

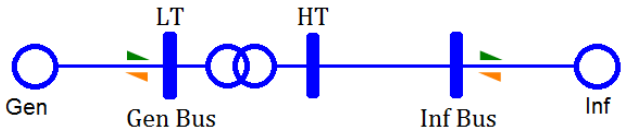

Figure 5.1 One-line diagram of simple network system

For the simulation, following specific models were selected from the PSS/E models; a GENROU model for a round-rotor typed machine (a synchronous generator), an On-Load Tap Changer (OLTC) model for a two-winding transformer and a GENCLS model for an infinite bus generator.

5.2.1. Model Data

In simulation, following three buses are used; a generator bus, an infinite bus, and a HT (High Tension or High Voltage) bus of a transformer. The detailed bus data on these buses are listed in Appendix A.1. This includes the values for the magnitude of voltage [pu], its angle [degree], and basic parameters determined by the system operation. Here, note that

‘Gen Bus’ has the bus type 2 which indicates a generator bus that either regulates voltage or has a fixed reactive power. The infinite bus has the bus type 3 that stands for a slack (or swing) bus which is used to provide for system losses by emitting or absorbing real and/or reactive power to and from the system. It was set a fixed voltage magnitude and angle as 1 [pu] and 0 degree respectively, and has a varying real/reactive power injection to satisfy overall real and reactive power balance.

Pertaining to the modeling of generators in PSS/E, a synchronous generator and an infinite bus generator were chosen respectively. For a synchronous generator, numerous parameters and characteristics were entered into the ‘Network data’ section. These data include real and reactive power supplied by a synchronous generator, minimum and the maximum value of real and reactive power, base unit, complex machine impedance and so on. The basic parameters of a generator are shown in Table 5.1, and all the detailed parameters of generators are listed in Appendix A.2.

Table 5.1 Parameters of a generator

No.	Parameters	Unit	Values
1	T'do (> 0)	s	9.25
2	T"do (> 0)	s	0.048
3	T'qo (> 0)	s	0.62
4	T"qo (> 0)	s	0.097
5	H	MW.s/MVA	6.705
6	D	p.u.	0.05
7	Xd	p.u.	1.87
8	Xq	p.u.	1.77
9	X'd	p.u.	0.21
10	X'q	p.u.	0.38
11	X"d = X"q	p.u.	0.155
12	Xl	p.u.	0.115

There is a branch that connects the HT bus of a two-winding transformer and an infinite bus. Here, the resistance is neglected and the line impedance is expressed in per unit. The values were set as same with that of transfer impedance (X_E) in Chapter 4 which is 0.00715 [pu].

The transformer in this case study was modeled as a two-winding transformer with an On-Load Tap Changer (OLTC) model and is connected between a generator bus and the HT bus of a transformer as shown Figure 5.1. The parameters contain the winding I/O code which specifies the units in which the turns ratio, the admittance I/O code that defines the units in which magnetizing admittances, the impedance data I/O code that specifies the units in which the winding impedances, the wind 1-ratio, the wind 2-ratio and so forth. All these detailed parameters are depicted in Appendix A.3.

5.2.2 Simulation Method

For the simulation of simple network system, a SMIB model, all the required characteristics and parameters on buses, branches and machines were entered into the 'Network data' tab in a 'Case' file. The real and reactive power supplied by a generator were calculated based on apparent power and power factor of each operating condition: 0.95 leading, unity and 0.8 lagging. Here, it was used 0.8 lagging of power factor for the chosen generator instead of the typical value, 0.85 lagging based on the specification of a synchronous generator from its manufacturer. The calculated values of real and reactive power are listed in Table 5.2. The one-line diagram was drawn as shown in Figure 5.1. Once these processes are done, it is solved the load flow solutions using 'Full Newton-Rapson method'. In a load flow simulation, the system is basically stabilized at one operating point. If this process has done properly, the message 'Zero mismatched MVA.' will be displayed in an 'Output Bar' window.

Table 5.2 Real and reactive power supplied by a generator

Cases	Operating Conditions	S [MVA]	P [MW]	Q [MVAR]
Case1	0.90 PF leading	153.83	138.447	-67.0529
Case2	0.91 PF leading	153.83	146.1385	-63.7792
Case3	0.95 PF leading	153.83	146.1385	-48.0334
Case4	1 Unity	153.83	-153.8	0
Case5	0.8 PF lagging	153.83	123.064	92.298

For the dynamics simulation, a dynamics file or a snapshot file that contains all the information of parameters for dynamics on machines such as generator, governor, exciter, and stabilizer is loaded. All the details on dynamics data are listed in Appendix A.4. By running the menu 'launching the NEVA eigenvalue analysis', the PSS/E converts all data for the modal analysis and perform the modal analysis that evaluates eigenvalues and damping ratios, and NEVA plots all modes graphically on a complex s-plane. The simulations for all three different cases were conducted based on the value of real and reactive power by different operating conditions like Table 5.2 in each iteration.

5.2.3 Simulation Result

A small signal stability is conducted by NEVA modal analysis. The eigenvalues are computed and all the modes are plotted on a complex s-plane. The result is summarized in Table 5.3 and Figure 5.2, and all the plotted graphs are depicted in Appendix A.5.

Table 5.3 Result of modal analysis for a SMIB model

Cases	Operating Conditions	σ [Np/s]	ω [rad/s]	ζ [%]	Freq. [Hz]
Case 1	0.90 PF leading	-0.407	8.350	-4.864	1.329
Case 2	0.91 PF leading	-0.429	8.372	-5.122	1.333
Case 3	0.95 PF leading	-0.549	8.470	-6.467	1.348
Case 4	1 Unity	-0.940	8.755	-10.677	1.393
Case 5	0.8 PF lagging	-1.461	9.421	-15.329	1.499

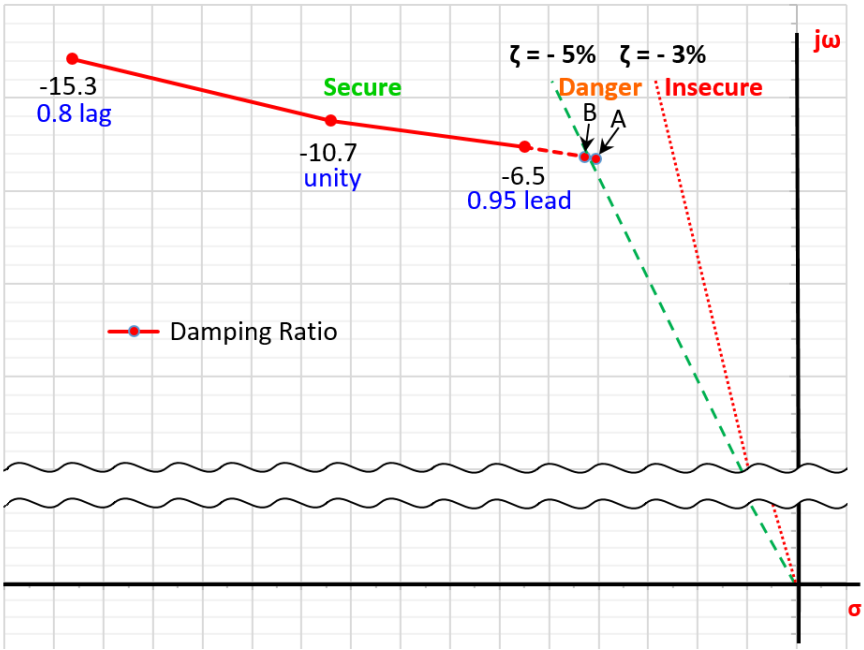

Figure 5.2 Trace of damping ratio of SMIB model

As shown in Table 5.3, the damping ratio (ζ) is -6.5% in 0.95 leading of power factor in operating condition of a generator, -10.7% in unity, and -15.3% in 0.8 lagging respectively. Herein, note that the NEVA software puts negative sign (-) in front of the value of damping ratio in order to indicate that the damping ratio is located on the left side of the imaginary axis. The damping ratios in the range of all operating conditions, from 0.95 leading via unity to 0.8 lagging, satisfy the condition that can ensure the small signal stability of power system which is 5% or higher of damping ratio as it is already examined in Chapter 4.4. The damping ratio was increased as the operating condition moves from 0.95 leading via unity to 0.8 lagging as it is expected.

As depicted in Figure 5.2, in order to qualify the small signal stability of power system the operating condition should be greater than 0.91 leading of power factor that is plotted as a point B in the graph. Obviously, if operating condition is 0.90 leading or lower, the damping ratio will be located in danger region which is regarded as weakly damped or insecure region that is considered as too weekly damped. Then this means that it can't be guaranteed the small signal stability of power system. Therefore, for the stability of power system the generator should be operated under the operating condition from 0.91 leading via unity to 0.8 lagging of power factor.

The decrement factor (σ) which is the real part of complex eigenvalue decides the axis of abscissas, and the damped natural frequency (ω) which is the imaginary part of complex eigenvalue signifies the axis ordinates in the complex s-plane. The decrement factor moves to the left and the damped natural frequency moves upward as the operation condition changes from leading via unity to lagging as can be seen in Figure 5.3. Obviously, the damping ratio which is composed of these two components increased as the operating condition changes from leading via unity to lagging as it is expected. This trend exactly matches with that of calculation from the theory in Chapter 4.

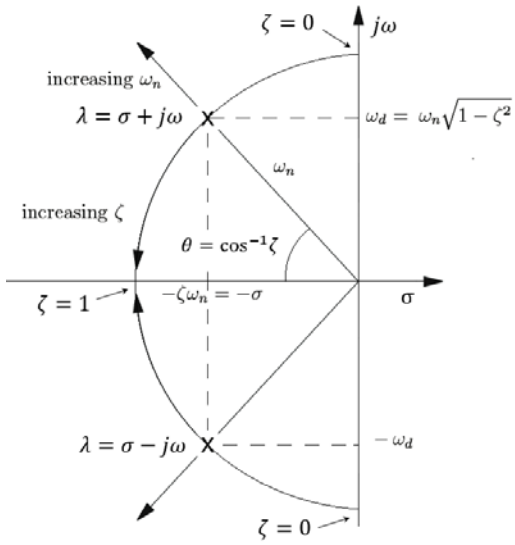

Figure 5.3 Complex conjugate pole in s-plane

Note that there are discrepancies in values of damping ratio between the theory and the simulation. It is regarded that these discrepancies mainly come from the difference of settings for the selected generator. In a simulation, governor, exciter and PSS are attached to the selected generator while they are not attached to a generating unit in the theory, and this influenced the damping ratio, that is much more enhanced it compared to the resultant values of calculation based on the theory. Overall, in spite of these minor discrepancies, by having same trend in changes of damping ratios, the theory which is suggested in Chapter 4 was corroborated by the result of simulation.

5.3. Persian Gulf Model

In the second scenario, the simulation has been expanded to the real-world power system. The power networks with selected four generating units are employed for the modeling in this scenario. The entire power systems of Persian Gulf area are composed of a great deal of generating units, plants, loads and so on, and they are interconnected one another with other neighboring power grids as shown in Figure 5.4 and 5.5. Figure 5.4 represents the power system of 400KV and Figure 5.5 stands for that of 220KV in Persian Gulf area respectively, and they are connected each other as well. Several new generating units will be newly added to the existing substations. As it is already discussed, the change of generation and loads will occur small disturbances which may bring the instability of power system ultimately if the damping is insufficient. Therefore, it is crucial to simulate and analyze the small signal stability so as to estimate the ability of real-world power system to return to a normal operating state after the small disturbances. It is also significantly important to ensure that the stability can be firmly secured through the enough damping over the entire plants and power grids.

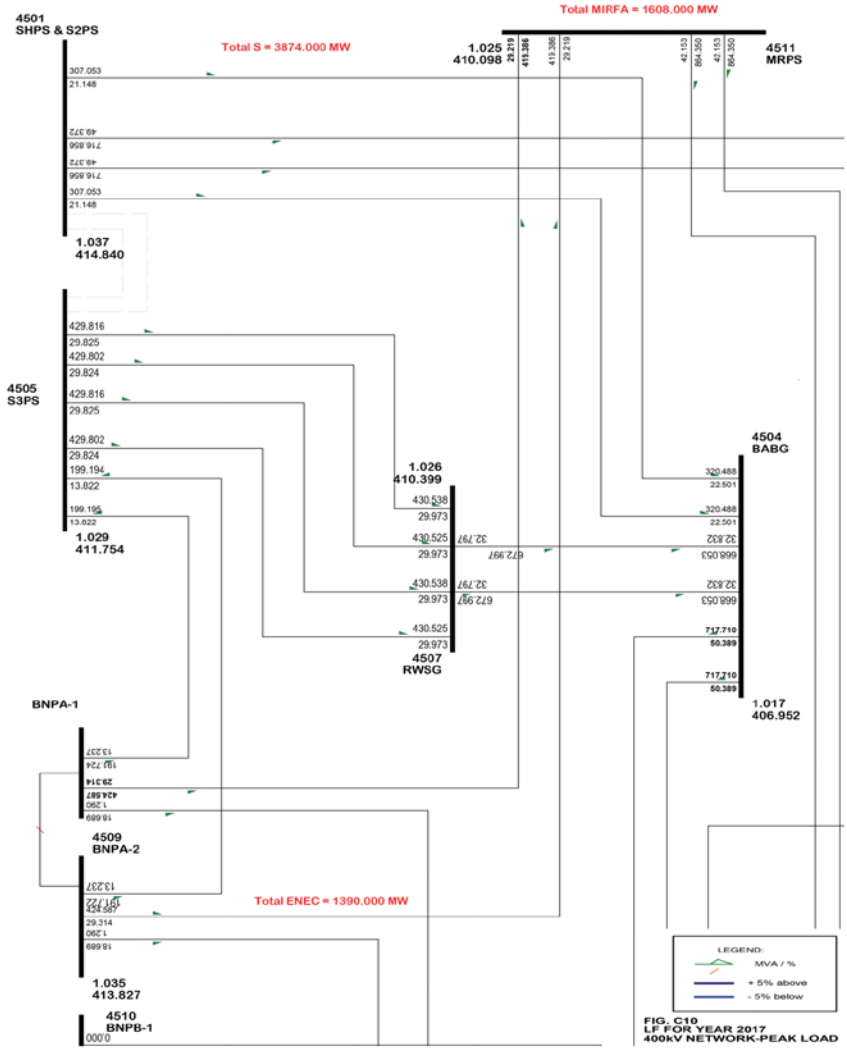

Figure 5.4 One-line diagram of 400KV in Gulf grid

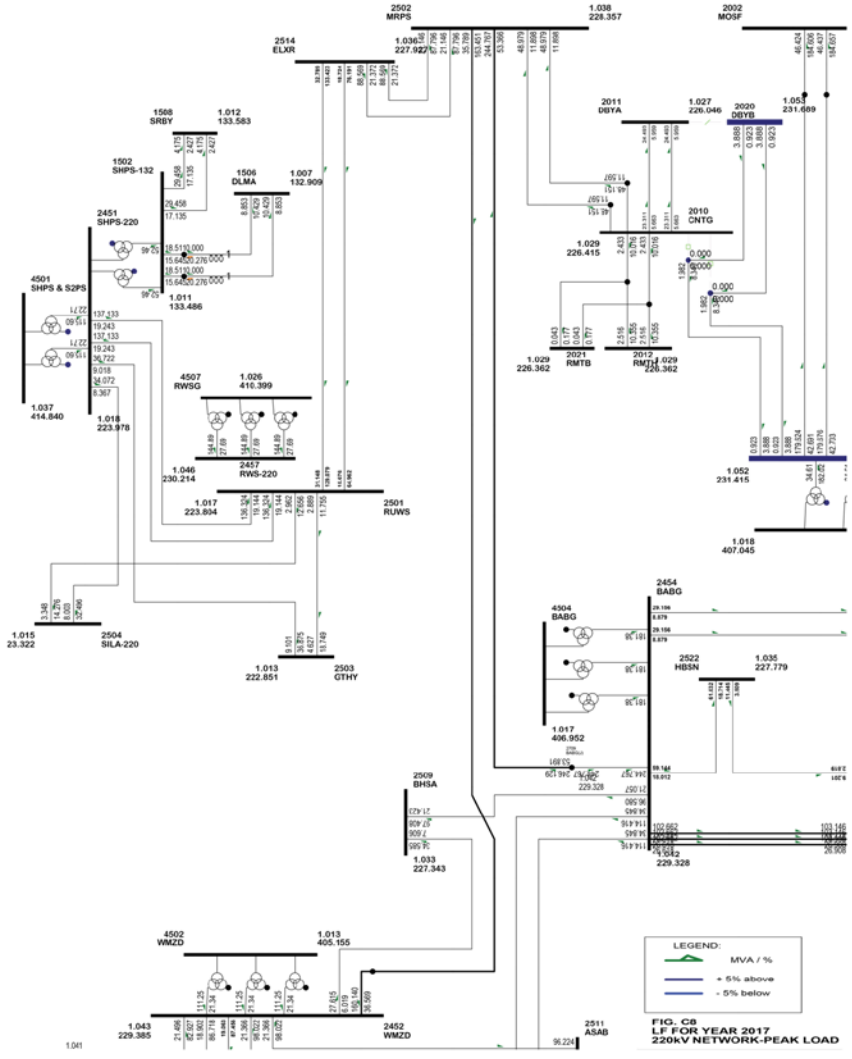

Figure 5.5 One-line diagram of 220KV in Gulf grid

5.3.1 Model Data

The voltage on each bus bar under normal operation varies from 400KV, 220KV and down to the lowest voltage 0.145KV. The detailed bus data are listed in Appendix B.1.

Currently in Persian Gulf grids many different types of existing generating units are interconnected with many other power grids. Four units of OCGT (Open cycle Gas Turbine) generators are setting up to a 400KV substation via two units of three winding step-up transformers. [21] The specification and parameters for each generator are described in Appendix B.2.

The real and reactive power supplied by each generator were determined based on the reactive capability curve as it is already discussed in Chapter 3. If the effect of turbine is ignored, the operating points that can generate maximum power output will be the points along the circular curve that starts from the point of 0.95 leading via unity to 0.8 lagging for the specified generators in this simulation. In this simulation, just like the SMIB model in the first simulation, 0.8 lagging was used for the maximum lagging operating condition of generator instead of the typical value, 0.85 lagging based on the specifications of generators from their manufacturer. The real and reactive power were calculated based on apparent power and each operating condition. The resultant values are same with Table 5.2.

The transformers in this simulation were modeled as two-winding step-up transformers with On-Load Tap Changer (OLTC) models and No-Load Tap Changer (NLTC) models and three-winding step-up transformers with OLTC models. All the detailed parameters for these transformers include type, capacity, impedance and X/R ratio are depicted in Appendix B.3.

5.3.2 Simulation Method

In the simulation of the Persian Gulf network system, all the neighboring interconnected power grids were converted into an infinite bus and the entire system was expressed to an equivalent circuit as a SMIB model like Figure 5.6 for the purpose of simplification in performing a small signal analysis.

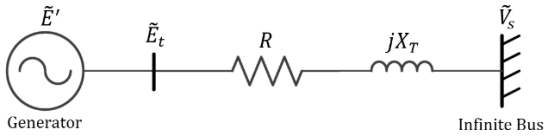

Figure 5.6 SMIB model

In order to get the data for the branch including line impedance, the infinite bus was connected to the 400KV bus bar of the given network. Accordingly, a three phase short circuit fault was applied on the entire power networks, thereby the Thévenin equivalent short circuit sequence impedances, i.e. transient positive impedance (Z1), transient negative

impedance (Z2) and transient zero impedance (Z0) on 400KV bus were computed respectively using PSS/E software. With transient positive short circuit impedance, the total impedance was calculated on the base of MVA. This equivalent impedance was used for the infinite bus with 400KV equivalent impedance model. An equivalent reduced model was created with these branch data and infinite bus data. Figure 5.7 shows the one-line diagram of this equivalent reduced model in Persian Gulf area.

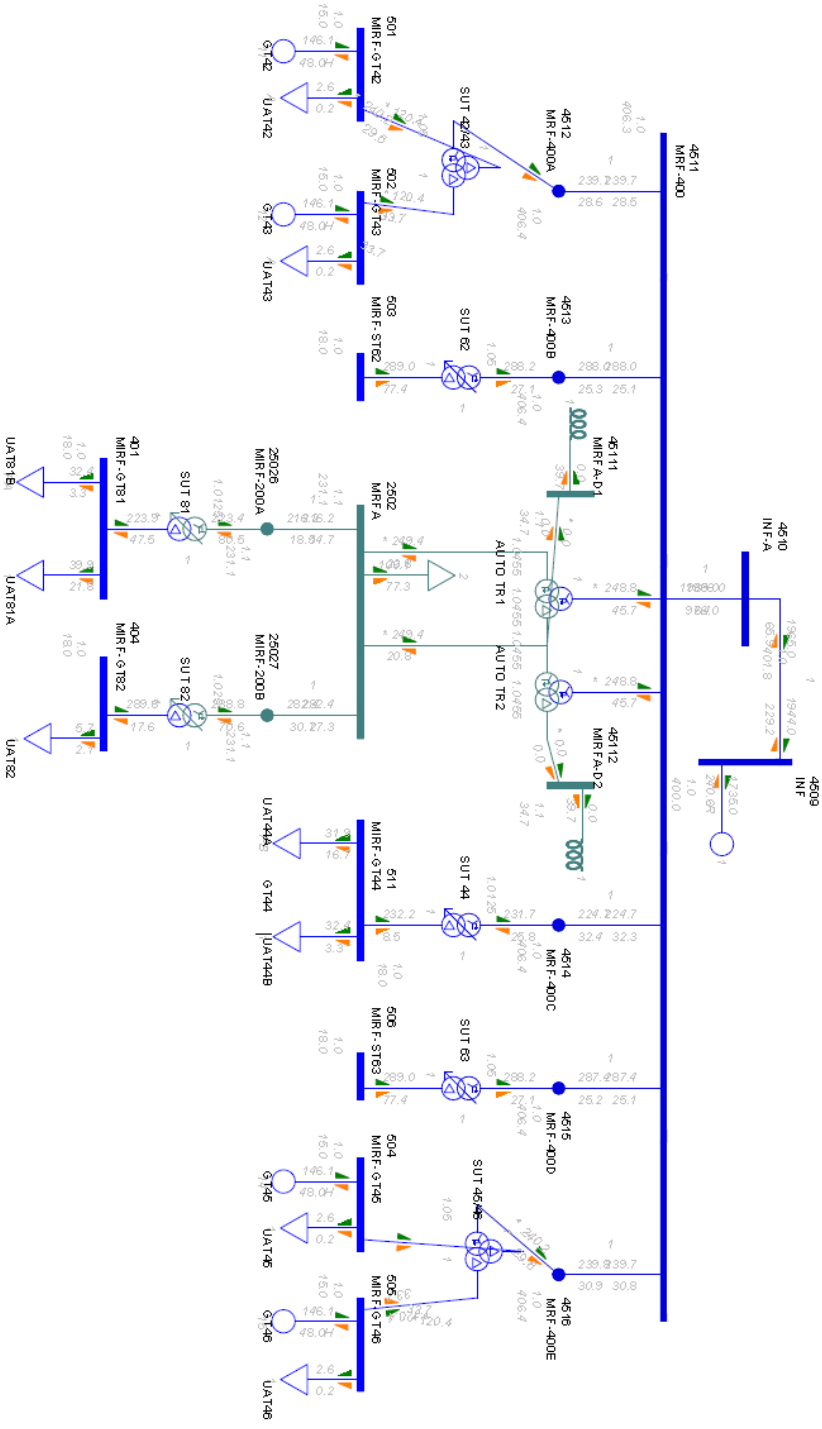

Figure 5.7 One-line diagram of equivalent reduced model

Likewise, all the required characteristics and parameters on bus, branch, machine, load, fixed shunt, switched shunt were entered in for the second simulation. Once it is solved the load flow solutions, the dynamics simulation was performed.

For the dynamics simulation, following dynamics models were selected like Table 5.4, and all the detailed dynamics data including parameters and block diagrams are depicted in Appendix A.4. In each iteration, the small signal analysis was performed based on different operating conditions to evaluate the effect of operating conditions on damping ratio.

Table 5.4 Dynamic models for the Persian Gulf power grid

Generator	Exciter	Governor	PSS
OCGT generator	IEEE EXAC2	GGOV1	IEEE PSS2B

5.3.3 Simulation Result

The eigenvalues are computed and all the modes are plotted on a complex s-plane using NEVA software. The result is summarized in Table 5.5 and all the plotted graphs are listed in Appendix B.4. As can be seen in the result in Table 5.5, the damping ratios of all generators were increased as the operating condition moves along the reactive capability curve i.e. 0.95 leading via unity to 0.8 lagging as it is expected. Note that the damping ratios in 0.95 leading and 0.99 leading of operating condition are below 5% which cannot satisfy the condition to ensure the small signal stability of

power system. Hence, each generator is desired not to operate in these operating conditions.

Table 5.5 Real and reactive power supplied by generators

Generator	PF	Sigma (σ) [Np/s]	Omega (ω) [rad/s]	Zeta (ζ) [%]	Frequency [Hz]
#501	0.95 leading	−0.179	6.9623	−2.5698	1.1081
	0.99 leading	−0.3227	7.2589	−4.4411	1.1553
	1 unity	−0.4788	7.4629	−6.4019	1.1878
	0.8 lagging	−0.9752	8.3303	−11.6278	1.3258
#502	0.95 leading	−0.179	6.9623	−2.5698	1.1081
	0.99 leading	−0.3226	7.2589	−4.4405	1.1553
	1 unity	−0.4788	7.4629	−6.4019	1.1878
	0.8 lagging	−0.9751	8.33	−11.6266	1.3258
#504	0.95 leading	−0.1274	6.9282	−2.5706	1.1082
	0.99 leading	−0.3228	7.2593	−4.4422	1.1554
	1 unity	−0.4789	7.4633	−6.403	1.1878
	0.8 lagging	−0.9752	8.3303	−11.6278	1.3258
#505	0.95 leading	−0.179	6.9628	−2.5706	1.1082
	0.99 leading	−0.3228	7.2593	−4.4422	1.1554
	1 unity	−0.4789	7.4633	−6.403	1.1878
	0.8 lagging	−0.9752	8.3303	−11.6278	1.3258

The change in damping ratio can be verified easily through the locus of on a graph intuitively as shown in Figure 5.8. The damping ratio is the parameter that represent the characteristic of amplitude attenuation and damping speed of oscillations following the small disturbances, and it is

expressed as the angle [%] between the isoline from an eigenvalue (mode) to the origin and the imaginary axis.

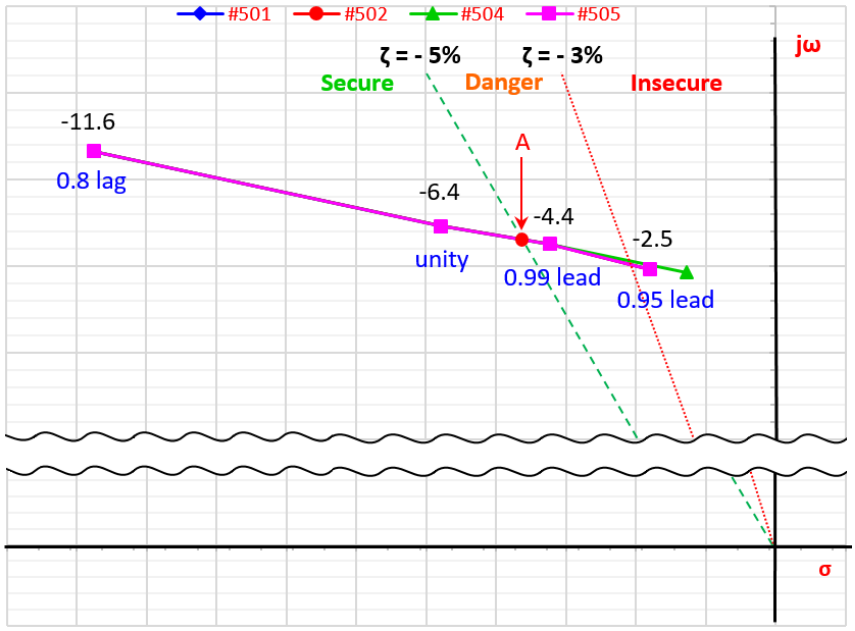

Figure 5.8 Trace of damping ratio of real-world network model

On a complex s-plane, it is desirable for swing mode, near the imaginary axis on the complex s-plane in the range of 0.6 to 18 and corresponding to the oscillation frequency from 0.1 to 3 [Hertz], to be placed on the left side of –5% isoline. [19] However, in Figure 5.8, the modes of each generator from 0.95 leading to the operating condition in the point A are placed in danger and insecure regions which are not desirable to ensure the small signal stability of power system. Therefore, for the purpose of stability of power system in whole Gulf grids, each generator should be operated in the rage from the operating condition of the point A to that of 0.8 lagging via unity.

5.4. Simulation Summary

In Chapter 5, in order to validate the effect of operating conditions of synchronous generators on damping ratios, two different scenarios were chosen and the simulation for small signal stability analysis were implemented using PSS/E software and its modulation NEVA.

In the first simulation, the small signal stability analysis was performed in a SMIB model. The calculated eigenvalues and plotted damping ratios on a complex s-plane showed that the damping ratios for the all range of operating conditions satisfy the condition to ensure the small signal stability in power system which is 5% or above in damping ratio. The damping ratio was increased as the operating condition moves from 0.95 leading via unity to 0.8 lagging of power factor.

In the second simulation, same analysis was performed in a real-world network with four generating units in Persian Gulf girds to test the ability to recover to a normal operating state after the small disturbances. The result revealed that the damping ratios from 0.95 leading of power factor to the operating condition of the point A of operating condition where the damping ratio is less than 5% didn't qualify the stability condition. On the other hand, the damping ratios from the operating condition of the point A to 0.8 lagging of power factor, that is the range of 5% or higher in damping ratio satisfied the condition for ensuring small signal stability in entire power system. In common with SMIB model, this model showed

same trend that the increase in damping ratio as the operating condition changes from 0.95 leading via unity to 0.8 lagging of power factor.

It is verified that most of the modes were placed in a secure region except the case of operating conditions from 0.95 leading to the point A where the damping ratio is less than 5% through a real-world network model simulation, and substantially improved damping of entire power system as the operating condition moves from leading via unity to lagging. It is also verified not only that the newly added generating units would not adversely affect the ambient power grids but also that small signal stability would be ensured over the entire power grids in the Persian Gulf area. As a result, the simulation on the power system in the Persian Gulf area also support the theory which is suggested in Chapter 4 by showing the same trend in the change of damping ratios.

Chapter 6. Conclusion

6.1. Conclusion

Small disturbances occur due to the change of generation or loads, and these inevitable disturbances should be controlled properly to maintain the stability of power system. Since small disturbances are mainly the result from insufficient damping of oscillation, it is crucial to improve damping. Naturally, many previous studies were focus on PSS controller in enhancing damping. However, the optimal tuning of PSS parameter is rather complicated and difficult in practice.

This paper shows that the operating condition of a generator also can have an impact on the damping ratio. Thereby, it is explained how to evaluate damping ratio theoretically most of all. The two principal constituent components of the damping ratio, synchronizing and damping torque coefficient were signified as a function of operating condition. That is, synchronizing torque coefficient was expressed as a function of real and reactive power, and the angle difference of transient emf and infinite voltage, and the damping torque coefficient as that of real and reactive power. These expressions enabled to understand the relationship between operating condition and synchronizing and damping torque coefficient.

The damping torque coefficient can be a variable along with different operating conditions. However, many previous approaches to evaluate damping ratio revealed the limit due to the damping torque

coefficient which is simply given as a constant or estimated through a complicated process. Instead, in this paper, it is calculated by the operating condition of a generator based on the operating points along the curve from leading via unity to lagging power factor that can generate maximum power output based on a reactive capability curve.

The impact of operating condition on damping ratio was verified with a simple network model and a practical power grid model with four generating units in the Persian Gulf area using PSS/E software. As expected in a mathematical theory, the results of small signal stability clearly demonstrated that the damping is enhanced as operating condition changes from leading via unity to lagging in both cases. It is showed that most of the modes were located in a secure region which can ensure the small signal stability with 5% or higher in damping ratio except some of leading operating conditions. In addition, it is verified that the newly added generating units will not have an adverse impact on their neighboring power grids as well as small signal stability will be guaranteed over the entire power networks.

As a summary, in this thesis, the effect of operating condition of a synchronous generator on damping ratio with mathematical equations and case studies with simulations were demonstrated. The damping ratio was expressed in terms of synchronizing and damping torque coefficient for the mathematical evaluation purpose. The range of operating condition of a synchronous generator was also modeled based on a reactive capability

curve. Lastly, in the simulations the analysis of small signal stability was conducted to support the mathematical theory. The result of simulations showed that the same trend on the change in damping ratio. As a result, the stability on power system was clearly verified through the simulations.

References

[1] R. Billinton, R. N. Allan, and L. Salvaderi, "Applied reliability assessment in electric power systems," 1991.

[2] NERC, "Bulk Power System Planning for Reliability," in *Reliability Assessment Guidebook* vol. Version 3.1, T. N. A. E. R. C. (NERC), Ed., ed. Atlanta, GA, 2012.

[3] P. Kundur *et al.*, "Definition and classification of power system stability IEEE/CIGRE joint task force on stability terms and definitions," *IEEE transactions on Power Systems,* vol. 19, no. 3, pp. 1387-1401, 2004.

[4] P. Kundur, N. J. Balu, and M. G. Lauby, *Power system stability and control*. McGraw-hill New York, 1994.

[5] M. Najafi and A. Kazemi, "Coordination of PSS and FACTS Damping Controllers in Large Power Systems for Dynamic Stability Improvement," in *2006 International Conference on Power System Technology*, 2006, pp. 1-6: IEEE.

[6] F. Liu, R. Yokoyama, Y. Zhou, and M. Wu, "Study on Oscillation Damping Effects of Power System Stabilizer with Eigenvalue Analysis Method for the Stability of Power Systems," *Modeling, Simulation and Identification ed. By Azah Mohamed, Sciyo,* 2010.

[7] F. P. Demello and C. Concordia, "Concepts of synchronous machine stability as affected by excitation control," *IEEE Transactions on power apparatus and systems,* vol. 88, no. 4, pp. 316-329, 1969.

[8] A. Jalilvand, M. D. Keshavarzi, and M. Khatibi, "Optimal tuning of PSS parameters for damping improvement using PSO algorithm," in *Power Engineering and Optimization Conference (PEOCO), 2010 4th International*, 2010, pp. 1-6: IEEE.

[9] C. Chennakesavan and P. Nalandha, "Multi-Machine Small Signal Stability Analysis For Large Scale Power System," *Indian Journal of Science and Technology,* vol. 7, no. S6, pp. 40-47, 2014.

[10] H. Ghasemi and C. Canizares, "On-line damping torque

estimation and oscillatory stability margin prediction," *IEEE Transactions on Power Systems,* vol. 22, no. 2, pp. 667-674, 2007.

[11] M. V. R. e. al, "Estimation of Damping Torque for Small-Signal Stability of Single Machine Infinite Bus System," *International Journal for Research in Applied Science & engineering Technology,* no. Special Issue-2, October

[12] "First Report of Power System Stability," *Transactions of the American Institute of Electrical Engineers,* vol. 56, no. 2, pp. 261-282, 1937.

[13] P. Kundur, "Introduction to the power system stability problem," *Power System Stability and Control, New York, McGraw-Hill, Inc,* pp. 17-35, 1994.

[14] E. Abu-Al-Feilat, N. Younan, and S. Grzybowski, "Estimating the synchronizing and damping torque coefficients using Kalman filtering," *Electric Power Systems Research,* vol. 52, no. 2, pp. 145-149, 1999.

[15] G. Wolansky and A. J. Zaslavski, *Variational and Optimal Control Problems on Unbounded Domains*. American Mathematical Soc., 2014.

[16] A. Von Meier, *Electric power systems: a conceptual introduction*. John Wiley & Sons, 2006.

[17] J. Machowski, J. Bialek, and J. Bumby, *Power system dynamics: stability and control*. John Wiley & Sons, 2011.

[18] U. A. B. e. al., *Electrical Machines - II*, 1st Edition ed. India: Technical Publications Pune, 2009.

[19] J. Norbury, "Assessment of System Warnings," in "Report to the Authority: Grid Code," National Grid, UK August 2015.

[20] O. Ruhle, Online Documentation NEVA PSS NETOMAC Eigenvalue Analysis, USA: Siemens AG, 2012. [Online].

[21] B.-H. Kim, "Small Signal Stability Study for PSS Tuning and System Damping," in "The Report on MIWPP Project: MIRFA IWPP Power Plant Model and Network Study," Korea 2016.

Appendix A. SMIB Model Data

A.1. Bus Data

Table A.1 Operating condition: 0.95 leading PF

Bus No.	Bus Name	Base kV	Code	Voltage (pu)	Angle (pu)	Normal V_{max} (pu)	Normal V_{min} (pu)
1	GEN BUS	18.0	-2	0.9163	6.06	1.1	0.9
2	INF BUS	400.0	3	1	0	1.1	0.9
3	HT	400.0	1	0.9960	0.62	1.1	0.9

Table A.2 Operating condition: unity PF

Bus No.	Bus Name	Base kV	Code	Voltage (pu)	Angle (pu)	Normal V_{max} (pu)	Normal V_{min} (pu)
1	GEN BUS	18.0	-2	0.9490	6.12	1.1	0.9
2	INF BUS	400.0	3	1	0	1.1	0.9
3	HT	400.0	1	0.9995	0.63	1.1	0.9

Table A.3 Operating condition: 0.8 lagging PF

Bus No.	Bus Name	Base kV	Code	Voltage (pu)	Angle (pu)	Normal V_{max} (pu)	Normal V_{min} (pu)
1	GEN BUS	18.0	-2	1.0083	4.53	1.1	0.9
2	INF BUS	400.0	3	1	0	1.1	0.9
3	HT	400.0	1	1.0061	0.48	1.1	0.9

A.2. Generator Data

Table A.4 Operating condition: 0.95 leading PF

Bus No.	Bus Name	Code	P_{Gen} (MW)	P_{Max} (MW)	P_{min} (MW)
1	GEN BUS	-2	146.1385	146.1385	146.1385
2	INF BUS	3	-145.7782	9999	-9999
Bus No.	**Q_{Gen} (Mvar)**	**Q_{Max} (Mvar)**	**Q_{min} (Mvar)**	**M_{base} (MVA)**	**R Source (pu)**
1	-48.0334	-48.0334	-48.0334	153.83	0.003875
2	65.6864	9999	-9999	99999	0
Bus No.	**X Source (pu)**	**R (pu)**	**Subtransient X (pu)**	**Transient X (pu)**	**Synchronous X (pu)**
1	0.155	0.003	0.12	0.19	1.87
2	1	0	1	1	1
Bus No.	**R-Negative (pu)**	**X-Negative (pu)**	**R-Zero (pu)**	**X-Zero (pu)**	**Grounding Z units**
1	0.019102	0.12	0.010201	0.085	Ohm
2	0	1	0	1	P.U.
Bus No.	**Grounding R**	**Grounding X**	**Reference Angle (deg)**		
1	487.1249	0	0		
2	**0**	**0**	**0**		

Table A.5 Operating condition: unity PF

Bus No.	Bus Name	Code	P_{Gen} (MW)	P_{Max} (MW)	P_{min} (MW)
1	GEN BUS	-2	153.8	153.8	153.8
2	INF BUS	3	-153.4941	9999	-9999
Bus No.	**Q_{Gen} (Mvar)**	**Q_{Max} (Mvar)**	**Q_{min} (Mvar)**	**M_{base} (MVA)**	**R Source (pu)**
1	0	0	0	153.83	0.003875
2	16.4552	9999	-9999	99999	0
Bus No.	**X Source (pu)**	**R (pu)**	**Subtransient X (pu)**	**Transient X (pu)**	**Synchronous X (pu)**
1	0.155	0.003	0.12	0.19	1.87
2	1	0	1	1	1
Bus No.	**R-Negative (pu)**	**X-Negative (pu)**	**R-Zero (pu)**	**X-Zero (pu)**	**Grounding Z units**
1	0.019102	0.12	0.010201	0.085	Ohm

2	0	1	0	1	P.U.

Bus No.	Grounding R	Grounding X	Reference Angle (deg)
1	487.1249	0	0
2	0	0	0

Table A.6 Operating condition: 0.8 lagging PF

Bus No.	Bus Name	Code	P_{Gen} (MW)	P_{Max} (MW)	P_{min} (MW)
1	GEN BUS	-2	123.0640	123.0640	123.0640
2	INF BUS	3	-122.7664	9999	-9999

Bus No.	Q_{Gen} (Mvar)	Q_{Max} (Mvar)	Q_{min} (Mvar)	M_{base} (MVA)	R Source (pu)
1	92.2980	92.2980	92.2980	153.83	0.003875
2	-77.7203	9999	-9999	99999	0

Bus No.	X Source (pu)	R (pu)	Subtransient X (pu)	Transient X (pu)	Synchronous X (pu)
1	0.155	0.003	0.12	0.19	1.87
2	1	0	1	1	1

Bus No.	R-Negative (pu)	X-Negative (pu)	R-Zero (pu)	X-Zero (pu)	Grounding Z units
1	0.019102	0.12	0.010201	0.085	Ohm
2	0	1	0	1	P.U.

Bus No.	Grounding R	Grounding X	Reference Angle (deg)
1	487.1249	0	0
2	0	0	0

A.3. Transformer Data

Table A.7 Two winding transformer

From Bus No.	From Bus Name	To Bus No.	To Bus Name	Name	Tap Positions
1	GEN BUS	3	HT BUS	2 Winding TR	33
Winding I/O Code	**Impedance I/O Code**	**Admittance I/O Code**	**Specified R (pu or watts)**	**Specified X (pu)**	**Rate1 (MVA)**
Turn ratio (pu on bus base kV)	Z pu (winding base)	Y pu (system base)	0.00313	0.1965	350
Rate2 (MVA)	**Rate3 (MVA)**	**Magnetizing G (pu or watts)**	**Magnetizing B (pu)**	**Winding MVA Base**	**Wind 1 Ratio (pu or kV)**
0	0	0	0	350	1.05
Wind 1 Nominal kV	**Wind 1 Angle**	**Wind 2 Ratio (pu or kV)**	**Wind 2 Nominal kV**	**R_{max} (pu, kV, deg)**	**R_{min} (pu, kV, deg)**
0	0	1	0	1.1	0.9
V_{max} (pu, kV, deg)	**V_{min}**	**R (table corrected pu or watts)**	**X (table corrected pu)**	**Vector Group**	**Connection Code**
1.1	0.9	0.00313	0.1965	YNd1	12 - No series path, ground winding 1

A.4. Dynamics Data

A.4.1. Generator 1 (for Gen Bus) – Model: GENROU

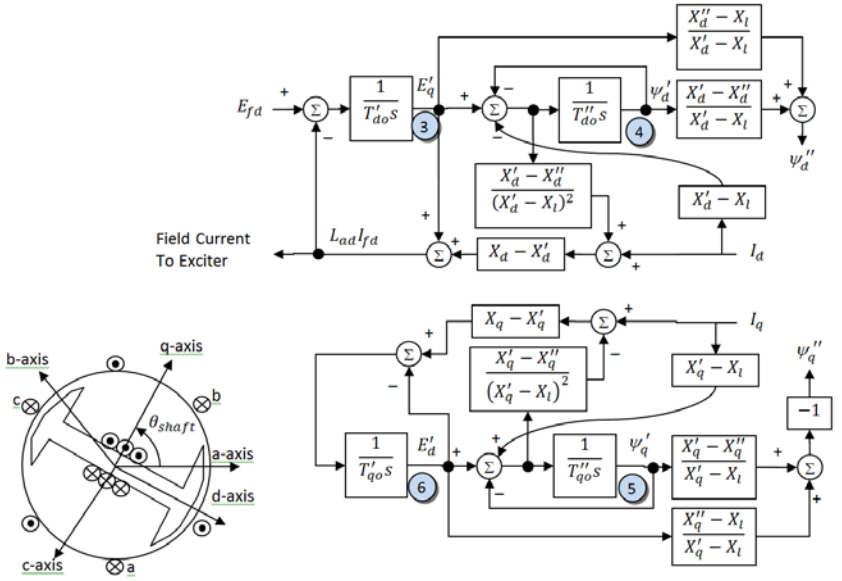

Figure A.1 Block diagram of a generator

Table A.8 Parameters of a generator

No.	parameters	Description	unit	values
1	T'_{do} (> 0)	Direct axis open circuit transient time constant	s	9.25
2	T''_{do} (> 0)	Direct axis open circuit sub-transient time constant	s	0.048
3	T'_{qo} (> 0)	Quadrature axis open circuit transient time constant	s	0.62
4	T''_{qo} (> 0)	Quadrature axis open circuit sub-transient time constant	s	0.097
5	H	Inertia	MW.s/MVA	6.705
6	D	Speed damping	p.u.	0.05
7	X_d	Direct axis reactance	p.u.	1.87
8	X_q	Quadrature axis reactance	p.u.	1.77
9	X'_d	Direct axis transient reactance	p.u.	0.21
10	X'_q	Quadrature axis transient reactance	p.u.	0.38
11	$X''_d = X''_q$	Direct/quadrature axis sub-transient reactance	p.u.	0.155
12	X_l	Leakage reactance	p.u.	0.115
13	S (1.0)	Saturation factor at 1.0 pu voltage		1.177
14	S (1.2)	Saturation factor at 1.2 pu voltage		1.838

A.4.2. Exciter – Model: IEEE EXAC2

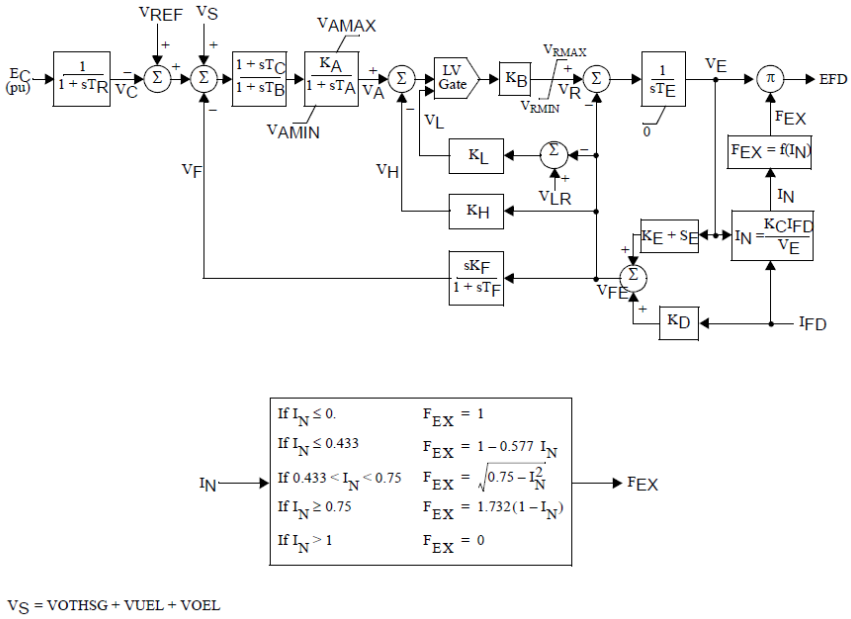

Figure A.2 Block diagram of an exciter

Table A.9 Parameters of an exciter

No.	Parameters	Description	Unit	Values
1	T_R	Voltage Transducer Time Constant	sec	0.01
2	T_B	Phase Lag Time Constant (s)	sec	1
3	T_C	Phase Lead Time Constant (s)	sec	1
4	K_A	AVR Gain		1000
5	T_A	AVR Time Constant	sec	0.01
6	V_{AMAX}	AVR Positive Limit		14.1
7	V_{AMIN}	AVR Negative Limit		-14.1
8	K_B	Gain		1
9	V_{RMAX}	FCR Positive Limit		14.1
10	V_{RMIN}	FCR Negative Limit		-14.1
11	T_E	Exciter Time Constant	sec	0.79
12	K_L	Current Limit Gain		4
13	K_H	Current Compensation		0
14	K_F	Rate Feedback Gain		0.05

15	T_F	Rate Feedback Time Constant	sec	1
16	K_C	Rectifier Commutation Factor		0.1
17	K_D	Load Factor		1.28
18	K_E	Alternator Gain		1
19	V_{LR}	Current Limit Set point		18.46
20	E_1	EFD at 75%		4.62
21	S_E (E_1)	Saturation Factor at E_{FD} 75%		0.02
22	E_2	E_{FD} max		6.16
23	S_E (E_2)	Saturation Factor at E_{FD} max		0.03

A.4.3. Governor – Model: GGOV1

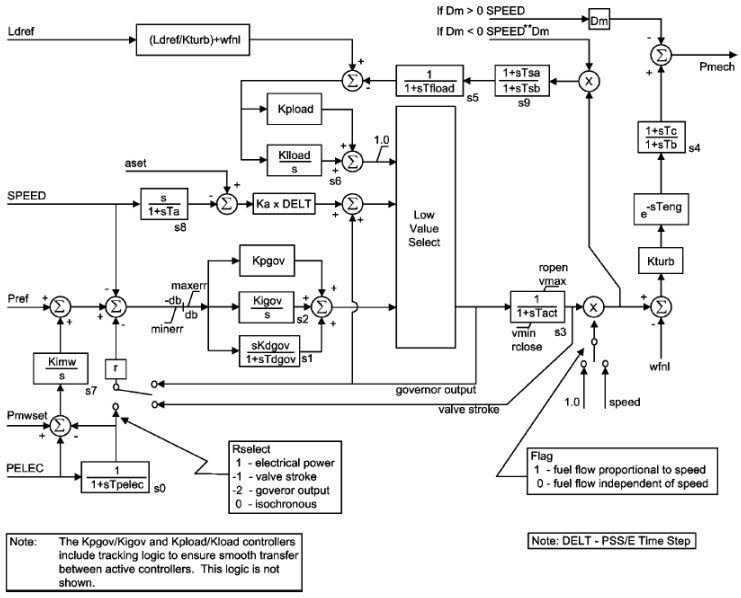

Figure A.3 Block diagram of a governor

Table A.10 Parameters of a governor

No.	Parameters	Description	Unit	Values
1	R	Permanent droop	pu	0.04
2	T_{pelec}	Electrical power transducer time constant	sec	1

3	max_{err}	Maximum value for speed error signal		0.05
4	min_{err}	Minimum value for speed error signal		-0.05
5	K_{pgov}	Governor proportional gain		10
6	K_{igov}	Governor integral gain		2
7	K_{dgov}	Governor derivative gain		0
8	T_{dgov}	Governor derivative controller time constant	sec	1
9	v_{max}	Maximum valve position limit		1
10	v_{min}	Minimum valve position limit		0.15
11	T_{act}	Actuator time constant	sec	0.5
12	K_{turb}	Turbine gain		1.5
13	W_{fnl}	No load fuel flow	pu	0.2
14	T_b	Turbine lag time constant	sec	0.1
15	T_c	Turbine lead time constant	sec	0
16	T_{eng}	Transport lag time constant for diesel engine	sec	0
17	T_{fload}	Load Limiter time constant	sec	3
18	K_{pload}	Load limiter proportional gain for PI controller		2
19	K_{iload}	Load limiter integral gain for PI controller		0.67
20	L_{dref}	Load limiter reference value	pu	1
21	D_m	Mechanical damping coefficient		0
22	R_{open}	Maximum valve opening rate	pu/sec	0.1
23	R_{close}	Maximum valve closing rate	pu/sec	-0.1
24	K_{imw}	Power controller (reset) gain		0
25	A_{set}	Acceleration limiter set point	pu/sec	0.01
26	K_a	Acceleration limiter gain		10
27	T_a	Acceleration limiter time constant	sec	0.1
28	T_{rate}	Turbine rating	MW	123
29	db	Speed governor dead band		0

30	T_{sa}	Temperature detection lead time constant	sec	4
31	T_{sb}	Temperature detection lag time constant	sec	5
32	R_{up}	Maximum rate of load limit increase		99
33	R_{down}	Maximum rate of load limit decrease		-99

A.4.4. PSS – Model: IEEE PSS2B

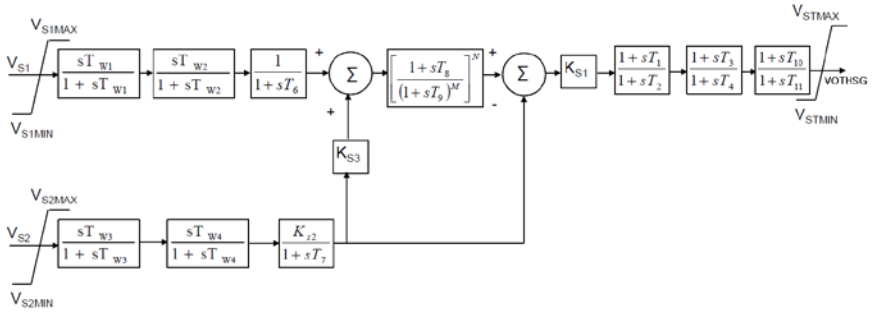

Figure A.4 Block diagram of a PSS

Table A.11 Parameters of a PSS

No.	Parameters	Description	Unit	Values
1	T_{w1}	Washout Time constant - Signal 1	sec	2
2	T_{w2}	Washout Time Constant - Signal 1	sec	2
3	T_6	Time Constant - Signal 1	sec	0
4	T_{w3}	Washout Time Constant - Signal 2	sec	2
5	T_{w4}	Washout Time Constant - Signal 2	sec	0
6	T_7	Lag Time Constant - Signal 2	sec	2
7	K_{S2}	Inertia Gain (=T_7/2H)		0.1491
8	K_{S3}	P_e Gain		1
9	T_8	Ramp Tracking Filter Lead Time Constant	sec	0.5
10	T_9	Ramp Tracking Filter Lag Time Constant	sec	0.1

11	K_{S1}	PSS Gain		20
12	T_1	Phase Lead Time Constant	sec	0.3
13	T_2	Phase Lag Time Constant	sec	0.025
14	T_3	Phase Lead Time Constant	sec	0.1
15	T_4	Phase Lag Time Constant	sec	0.015
16	T_{10}	Phase Lead Time Constant	sec	0
17	T_{11}	Phase Lag Time Constant	sec	0
18	V_{S1MAX}	Stabilizer Input Maximum, Input 1		2.5
19	V_{S1MIN}	Stabilizer Input Minimum, Input 1		-2.5
20	V_{S2MAX}	Stabilizer Input Maximum, Input 2		2.5
21	V_{S2MIN}	Stabilizer Input Minimum, Input 2		-2.5
22	V_{STMAX}	Positive Output Limit	pu	0.1
23	V_{STMIN}	Negative Output Limit	pu	-0.1

A.5. Simulation Result for SMIB Model

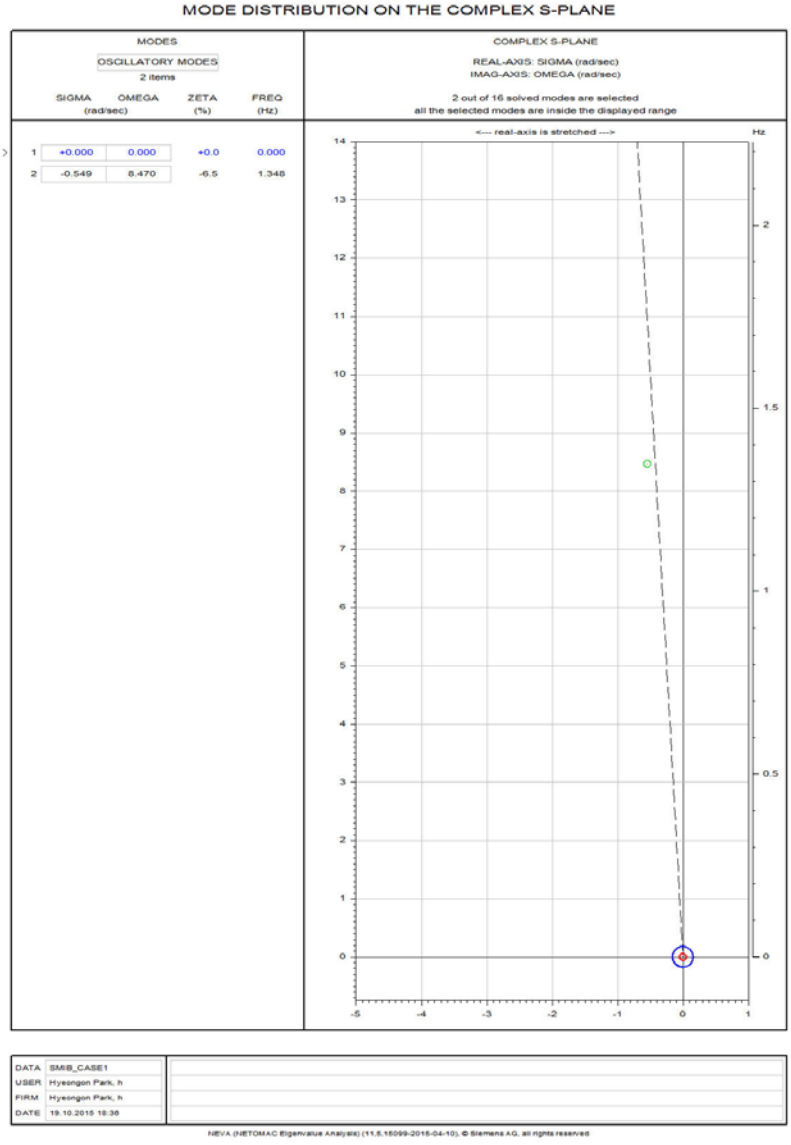

Figure A.5 Operating condition: 0.95 leading PF

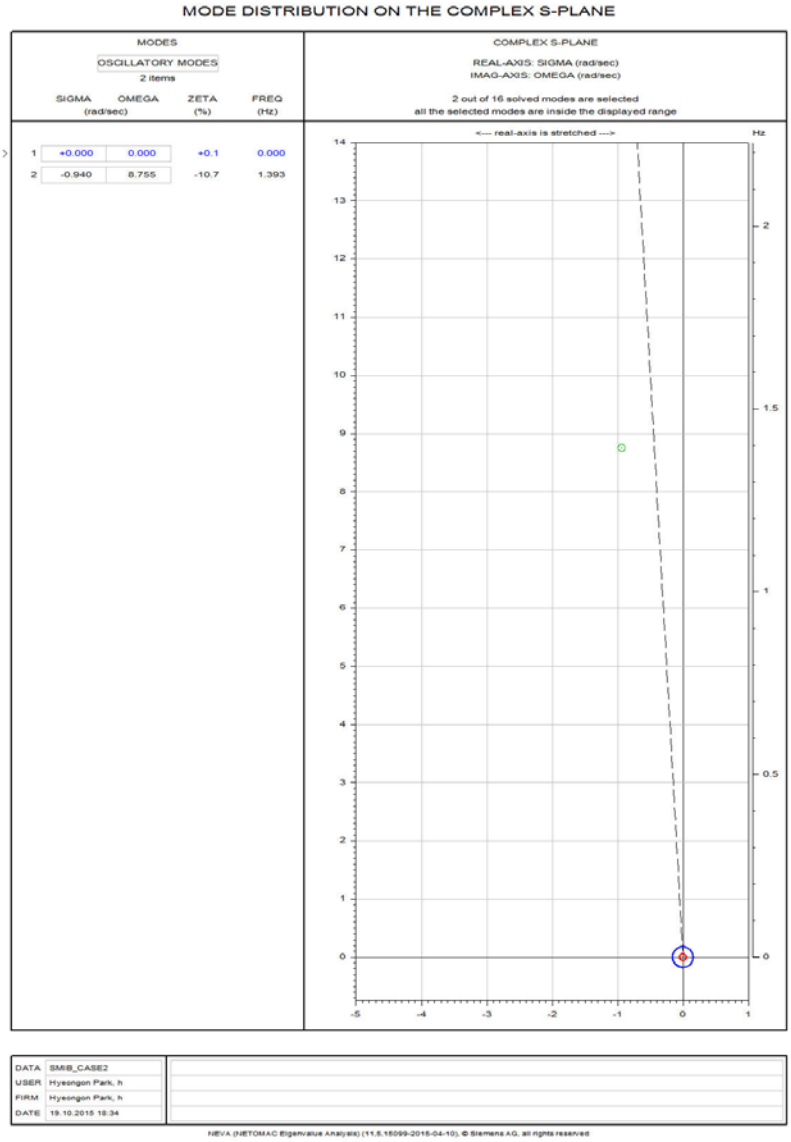

Figure A.6 Operating condition: unity PF

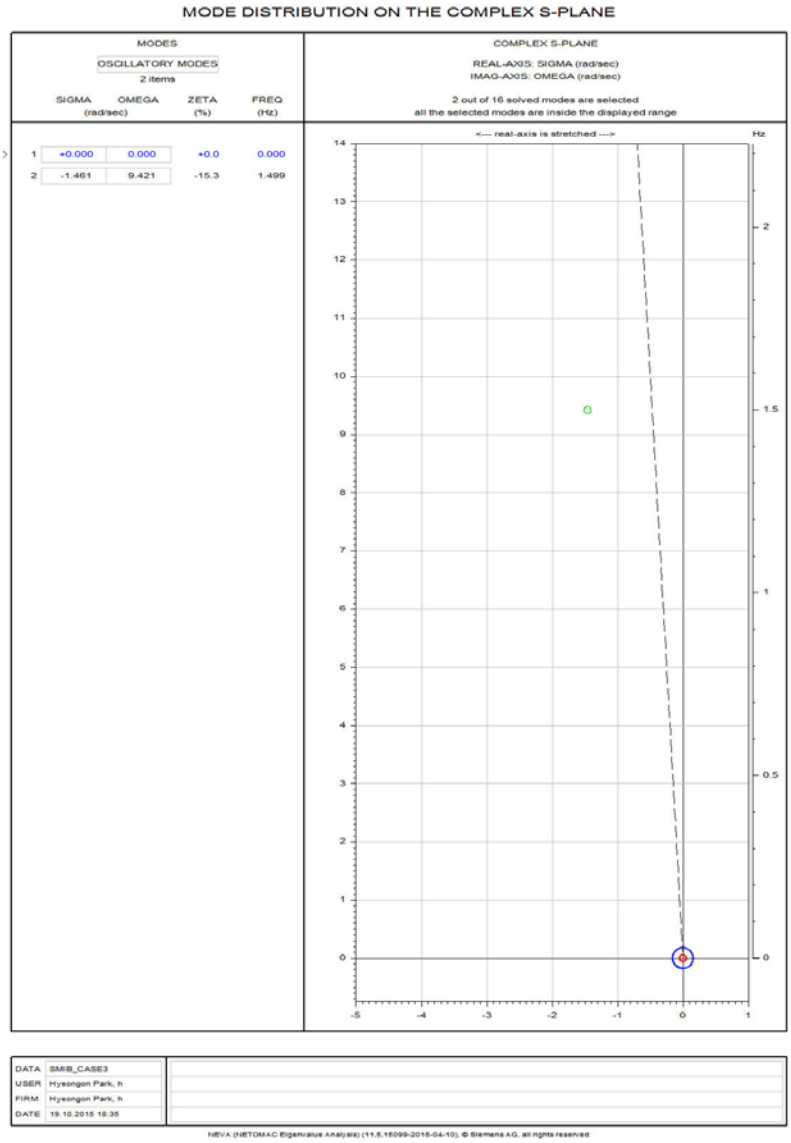

Figure A.7 Operating condition: 0.8 lagging PF

Appendix B. Real-World Network Model Data

B.1. Bus Data

Table B.1 Operating condition: 0.95 leading PF

Bus No.	Bus Name	Base kV	Code	Voltage (pu)	Angle (pu)	Normal Vmax (pu)	Normal Vmin (pu)
401	MIRF-GT81	18.0	1	0.9241	-3.41	1.1	0.9
404	MIRF-GT82	18.0	1	0.9304	-1.00	1.1	0.9
501	MIRF-GT42	15.0	-2	0.8132	15.75	1.1	0.9
502	MIRF-GT43	15.0	-2	0.8132	15.75	1.1	0.9
503	MIRF-ST62	18.0	1	0.9071	2.01	1.1	0.9
504	MIRF-GT45	15.0	-2	0.8132	15.74	1.1	0.9
505	MIRF-GT46	15.0	-2	0.8132	15.74	1.1	0.9
506	MIRF-ST63	18.0	1	0.9071	2.01	1.1	0.9
511	MIRF-GT44	18.0	1	0.9252	-0.68	1.1	0.9
2502	MRFA	220.0	1	0.9552	-0.64	1.1	0.9
4509	INF	400.0	3	1	0	1.1	0.9
4510	INF-A	400.0	1	0.9761	0.98	1.1	0.9
4511	MRF-400	400.0	1	0.9525	2.01	1.1	0.9
4512	MRF-400A	400.0	1	0.9521	2.05	1.1	0.9
4513	MRF-400B	400.0	1	0.9525	2.01	1.1	0.9
4514	MRF-400C	400.0	1	0.9524	2.00	1.1	0.9
4515	MRF-400D	400.0	1	0.9525	2.01	1.1	0.9
4516	MRF-400E	400.0	1	0.9522	2.05	1.1	0.9
25026	MIRF-200A	220.0	1	0.9550	-0.43	1.1	0.9
25027	MIRF-200B	220.0	1	0.9552	-0.41	1.1	0.9
45111	MIRFA-D1	33.0	1	0.9190	-0.51	1.1	0.9
45112	MIRFA-D2	33.0	1	0.9190	-0.51	1.1	0.9

Table B.2 Operating condition: unity PF

Bus No.	Bus Name	Base kV	Code	Voltage (pu)	Angle (pu)	Normal Vmax (pu)	Normal Vmin (pu)
401	MIRF-GT81	18.0	1	0.9467	-3.19	1.1	0.9
404	MIRF-GT82	18.0	1	0.9522	-0.56	1.1	0.9
501	MIRF-GT42	15.0	-2	0.9083	14.56	1.1	0.9
502	MIRF-GT43	15.0	-2	0.9083	14.56	1.1	0.9
503	MIRF-ST62	18.0	1	0.9271	1.98	1.1	0.9
504	MIRF-GT45	15.0	-2	0.9083	14.56	1.1	0.9
505	MIRF-GT46	15.0	-2	0.9083	14.56	1.1	0.9
506	MIRF-ST63	18.0	1	0.9071	1.98	1.1	0.9
511	MIRF-GT44	18.0	1	0.9463	-0.60	1.1	0.9
2502	MRFA	220.0	1	0.9775	-0.33	1.1	0.9
4509	INF	400.0	3	1	0	1.1	0.9
4510	INF-A	400.0	1	0.9866	0.98	1.1	0.9
4511	MRF-400	400.0	1	0.9735	1.98	1.1	0.9
4512	MRF-400A	400.0	1	0.9734	2.02	1.1	0.9
4513	MRF-400B	400.0	1	0.9735	1.98	1.1	0.9
4514	MRF-400C	400.0	1	0.9734	1.97	1.1	0.9
4515	MRF-400D	400.0	1	0.9735	1.98	1.1	0.9
4516	MRF-400E	400.0	1	0.9734	2.01	1.1	0.9
25026	MIRF-200A	220.0	1	0.9773	-0.35	1.1	0.9
25027	MIRF-200B	220.0	1	0.9775	-0.33	1.1	0.9
45111	MIRFA-D1	33.0	1	0.9405	-0.43	1.1	0.9
45112	MIRFA-D2	33.0	1	0.9405	-0.43	1.1	0.9

Table B.3 Operating condition: 0.8 lagging PF

Bus No.	Bus Name	Base kV	Code	Voltage (pu)	Angle (pu)	Normal Vmax (pu)	Normal Vmin (pu)
401	MIRF-GT81	18.0	1	0.9829	-3.74	1.1	0.9
404	MIRF-GT82	18.0	1	0.9873	-1.29	1.1	0.9
501	MIRF-GT42	15.0	-2	1.0578	9.32	1.1	0.9
502	MIRF-GT43	15.0	-2	1.0578	9.23	1.1	0.9
503	MIRF-ST62	18.0	1	0.9594	1.07	1.1	0.9
504	MIRF-GT45	15.0	-2	1.0578	9.23	1.1	0.9
505	MIRF-GT46	15.0	-2	1.0578	9.23	1.1	0.9
506	MIRF-ST63	18.0	1	0.9594	1.07	1.1	0.9
511	MIRF-GT44	18.0	1	0.9804	-1.33	1.1	0.9
2502	MRFA	220.0	1	1.0134	-1.08	1.1	0.9
4509	INF	400.0	3	1	0	1.1	0.9
4510	INF-A	400.0	1	1.0036	0.54	1.1	0.9
4511	MRF-400	400.0	1	1.0073	1.07	1.1	0.9
4512	MRF-400A	400.0	1	1.0077	1.10	1.1	0.9
4513	MRF-400B	400.0	1	1.0073	1.07	1.1	0.9
4514	MRF-400C	400.0	1	1.0073	1.06	1.1	0.9
4515	MRF-400D	400.0	1	1.0073	1.07	1.1	0.9
4516	MRF-400E	400.0	1	1.0076	1.09	1.1	0.9
25026	MIRF-200A	220.0	1	1.0133	-1.10	1.1	0.9
25027	MIRF-200B	220.0	1	1.0134	-1.08	1.1	0.9
45111	MIRFA-D1	33.0	1	0.9752	-1.17	1.1	0.9
45112	MIRFA-D2	33.0	1	0.9752	-1.17	1.1	0.9

B.2. Generator Data

Table B.4 Operating condition: 0.95 leading PF

Bus No.	Bus Name	Code	P_{Gen} (MW)	P_{Max} (MW)	P_{min} (MW)
501	MIRF-GT42	-2	146.1385	146.1385	146.1385
502	MIRF-GT43	-2	146.1385	146.1385	146.1385
504	MIRF-GT44	-2	146.1385	146.1385	146.1385
505	MIRF-GT45	-2	146.1385	146.1385	146.1385
4509	INF	3	-313.982	9999	-9999

Bus No.	Q_{Gen} (Mvar)	Q_{Max} (Mvar)	Q_{min} (Mvar)	M_{base} (MVA)	R Source (pu)
501	-48.0334	-48.0334	-48.0334	153.83	0.003875
502	-48.0334	-48.0334	-48.0334	153.83	0.003875
504	-48.0334	-48.0334	-48.0334	153.83	0.003875
505	-48.0334	-48.0334	-48.0334	153.83	0.003875
4509	604.8358	9999	-9999	99999	0

Bus No.	X Source (pu)	R (pu)	Subtransient X (pu)	Transient X (pu)	Synchronous X (pu)
501	0.155	0.003	0.12	0.19	1.87
502	0.155	0.003	0.12	0.19	1.87
504	0.155	0.003	0.12	0.19	1.87
505	0.155	0.003	0.12	0.19	1.87
4509	1	0	1	1	1

Bus No.	R-Negative (pu)	X-Negative (pu)	R-Zero (pu)	X-Zero (pu)	Grounding Z units
501	0.019102	0.12	0.010201	0.085	Ohm
502	0.019102	0.12	0.010201	0.085	Ohm
504	0.019102	0.12	0.010201	0.085	Ohm
505	0.019102	0.12	0.010201	0.085	Ohm
4509	0	1	0	1	P.U.

Bus No.	Grounding R	Grounding X	Reference Angle (deg)
501	487.1249	0	0
502	487.1249	0	0
504	487.1249	0	0
505	487.1249	0	0
4509	487.1249	0	0

Table B.5 Operating condition: unity PF

Bus No.	Bus Name	Code	P_{Gen} (MW)	P_{Max} (MW)	P_{min} (MW)
501	MIRF-GT42	-2	153.83	153.83	153.83
502	MIRF-GT43	-2	153.83	153.83	153.83
504	MIRF-GT44	-2	153.83	153.83	153.83
505	MIRF-GT45	-2	153.83	153.83	153.83
4509	INF	3	-313.982	9999	-9999

Bus No.	Q_{Gen} (Mvar)	Q_{Max} (Mvar)	Q_{min} (Mvar)	M_{base} (MVA)	R Source (pu)
501	0	0	0	153.83	0.003875
502	0	0	0	153.83	0.003875
504	0	0	0	153.83	0.003875
505	0	0	0	153.83	0.003875
4509	604.8358	9999	-9999	99999	0

Bus No.	X Source (pu)	R (pu)	Subtransient X (pu)	Transient X (pu)	Synchronous X (pu)
501	0.155	0.003	0.12	0.19	1.87
502	0.155	0.003	0.12	0.19	1.87
504	0.155	0.003	0.12	0.19	1.87
505	0.155	0.003	0.12	0.19	1.87
4509	1	0	1	1	1

Bus No.	R-Negative (pu)	X-Negative (pu)	R-Zero (pu)	X-Zero (pu)	Grounding Z units
501	0.019102	0.12	0.010201	0.085	Ohm
502	0.019102	0.12	0.010201	0.085	Ohm
504	0.019102	0.12	0.010201	0.085	Ohm
505	0.019102	0.12	0.010201	0.085	Ohm
4509	0	1	0	1	P.U.

Bus No.	Grounding R	Grounding X	Reference Angle (deg)
501	487.1249	0	0
502	487.1249	0	0
504	487.1249	0	0
505	487.1249	0	0
4509	487.1249	0	0

Table B.6 Operating condition: 0.8 lagging PF

Bus No.	Bus Name	Code	P_{Gen} (MW)	P_{Max} (MW)	P_{min} (MW)
501	MIRF-GT42	-2	123.0640	123.0640	123.0640
502	MIRF-GT43	-2	123.0640	123.0640	123.0640
504	MIRF-GT44	-2	123.0640	123.0640	123.0640
505	MIRF-GT45	-2	123.0640	123.0640	123.0640
4509	INF	3	-227.4724	9999	-9999

Bus No.	Q_{Gen} (Mvar)	Q_{Max} (Mvar)	Q_{min} (Mvar)	M_{base} (MVA)	R Source (pu)
501	-48.0334	-48.0334	-48.0334	153.83	0.003875
502	-48.0334	-48.0334	-48.0334	153.83	0.003875
504	-48.0334	-48.0334	-48.0334	153.83	0.003875
505	-48.0334	-48.0334	-48.0334	153.83	0.003875
4509	-54.8610	9999	-9999	99999	0

Bus No.	X Source (pu)	R (pu)	Subtransient X (pu)	Transient X (pu)	Synchronous X (pu)
501	0.155	0.003	0.12	0.19	1.87
502	0.155	0.003	0.12	0.19	1.87
504	0.155	0.003	0.12	0.19	1.87
505	0.155	0.003	0.12	0.19	1.87
4509	1	0	1	1	1

Bus No.	R-Negative (pu)	X-Negative (pu)	R-Zero (pu)	X-Zero (pu)	Grounding Z units
501	0.019102	0.12	0.010201	0.085	Ohm
502	0.019102	0.12	0.010201	0.085	Ohm
504	0.019102	0.12	0.010201	0.085	Ohm
505	0.019102	0.12	0.010201	0.085	Ohm
4509	0	1	0	1	P.U.

Bus No.	Grounding R	Grounding X	Reference Angle (deg)
501	487.1249	0	0
502	487.1249	0	0
504	487.1249	0	0
505	487.1249	0	0
4509	487.1249	0	0

B.3. Transformer Data

Table B.7 Two winding transformers

From Bus No.	From Bus Name	To Bus No.	To Bus Name	Name	Tap Positions
401	MIRF-GT81	25026	MIRF-200A	SUT 81	33
404	MIRF-GT82	25027	MIRF-200B	SUT82	33
503	MIRF-ST62	4513	MRF-400B	SUT 62	33
506	MIRF-ST63	4515	MRF-400D	SUT 63	33
511	MIRF-GT44	4514	MRF-400C	SUT 44	33

Winding I/O Code	Impedance I/O Code	Admittance I/O Code	Specified R (pu or watts)	Specified X (pu)	Rate1 (MVA)
Turn ratio (pu on bus base kV)	Z pu (winding base)	Y pu (system base)	0.003200	0.2203	350
Turn ratio (pu on bus base kV)	Z pu (winding base)	Y pu (system base)	0.003200	0.2203	350
Turn ratio (pu on bus base kV)	Z pu (winding base)	Y pu (system base)	0.003130	0.1965	350
Turn ratio (pu on bus base kV)	Z pu (winding base)	Y pu (system base)	0.003130	0.1965	350
Turn ratio (pu on bus base kV)	Z pu (winding base)	Y pu (system base)	0.003400	0.223	350

Rate2 (MVA)	Rate3 (MVA)	Magnetizing G (pu or watts)	Magnetizing B (pu)	Winding MVA Base	Wind 1 Ratio (pu or kV)
0	0	0	0	350	1.0125
0	0	0	0	350	1.0250
0	0	0	0	350	1.0500
0	0	0	0	350	1.0500
0	0	0	0	350	1.0125

Wind 1 Nominal kV	Wind 1 Angle	Wind 2 Ratio (pu or kV)	Wind 2 Nominal kV	Rmax (pu, kV, deg)	Rmin (pu, kV, deg)
0	0	1	0	1.1	0.9
0	0	1	0	1.1	0.9
0	0	1	0	1.1	0.9
0	0	1	0	1.1	0.9
0	0	1	0	1.1	0.9

Vmax (pu, kV, deg)	Vmin	R (table corrected pu or watts)	X (table corrected pu)	Vector Group	Connection Code

1.1	0.9	0.00320	0.22030	YNd1	12 - No series path, ground winding 1
1.1	0.9	0.00320	0.22030	YNd1	12 - No series path, ground winding 1
1.1	0.9	0.00313	0.19650	YNd1	12 - No series path, ground winding 1
1.1	0.9	0.00313	0.19650	YNd1	12 - No series path, ground winding 1
1.1	0.9	0.00324	0.22300	YNd1	12 - No series path, ground winding 1

Leakage impedance I/O code	Grounding Impedance I/O code	RG1	XG1	R01 (pu)	X01 (pu)
Z pu (winding base)	Ohms	0	0	0.002336	0.161173
Z pu (winding base)	Ohms	0	0	0.002336	0.161169
Z pu (winding base)	Ohms	0	0	0.002349	0.148004
Z pu (winding base)	Ohms	0	0	0.002349	0.148004
Z pu (winding base)	Ohms	0	0	0.002580	0.162555

Table B.8 Three winding transformers

From Bus No.	From Bus Name	To Bus No.	To Bus Name	Last Bus Number	Last Bus Name
501	MIRF-GT42	4512	MRF-400A	502	MIRF-GT43
504	MIRF-GT45	4516	MRF-400E	505	MIRF-GT46
4511	MRF-400	2502	MRFA	45111	MIRFA-D1
4511	MRF-400	2502	MRFA	45112	MIRFA-D2

Name	Non-metered end	Winding I/O Code	Impedance I/O Code	Admittance I/O Code	W1-2 R (pu or watts)
SUT 42/43	To bus	Turns ratio (pu)	Z pu (winding base)	Y pu (system base)	0.006450

SUT 45/46	To bus	Turns ratio (pu)	Z pu (winding base)	Y pu (system base)	0.006450
AUTO TR1	To bus	Turns ratio (pu)	Z pu (winding base)	Y pu (system base)	0.004443
AUTO TR2	To bus	Turns ratio (pu)	Z pu (winding base)	Y pu (system base)	0.004443

W1-2 X (pu)	W2-3 R (pu or watts)	W2-3 X (pu)	W3-1 R (pu or watts)	W3-1 X (pu)	Magnetizing G (pu or watts)
0.340200	0.006450	0.340200	0.012412	0.620776	0
0.340200	0.006450	0.340200	0.012412	0.620776	0
0.199951	0.002599	0.116971	0.003843	0.172957	0
0.199951	0.002599	0.116971	0.003843	0.172957	0

Magnetizing B (pu)	Winding 1-2 MVA Base	Winding 2-3 MVA Base	Winding 3-1 MVA Base	Impedance Adjustment Code	Star Bus Bus
0	306	306	306	Winding impedance	0.97386
0	306	306	306	Winding impedance	0.97382
0	500	125	125	Winding impedance	0.96806
0	500	125	125	Winding impedance	0.96806

Star Bus Angle	Vector Group	Connection Code	User Code	Leakage impedance I/O code	Grounding impedance I/O code
2.5	D1yn0d1	13 (3-1-3)	313	Z pu (winding base)	Ohms
2.5	D1yn0d1	13 (3-1-3)	313	Z pu (winding base)	Ohms
-1.2	YN0yn0d1	2 (1-1-3)	113	Z pu (winding base)	Z pu (system base)
-1.2	YN0yn0d1	2 (1-1-3)	113	Z pu (winding base)	Z pu (system base)

R01 (pu)	X01 (pu)	R02 (pu)	X02 (pu)	R03 (pu)	X03 (pu)
0.011610	0.612360	0.011610	0.612360	0.022341	1.117400
0.011610	0.612360	0.011610	0.612360	0.022341	1.117400
0.001600	0.071982	0.003743	0.168438	0.005535	0.249059
0.001600	0.071982	0.003743	0.168438	0.005535	0.249059

B.4. Simulation Result for Real-World Network Model

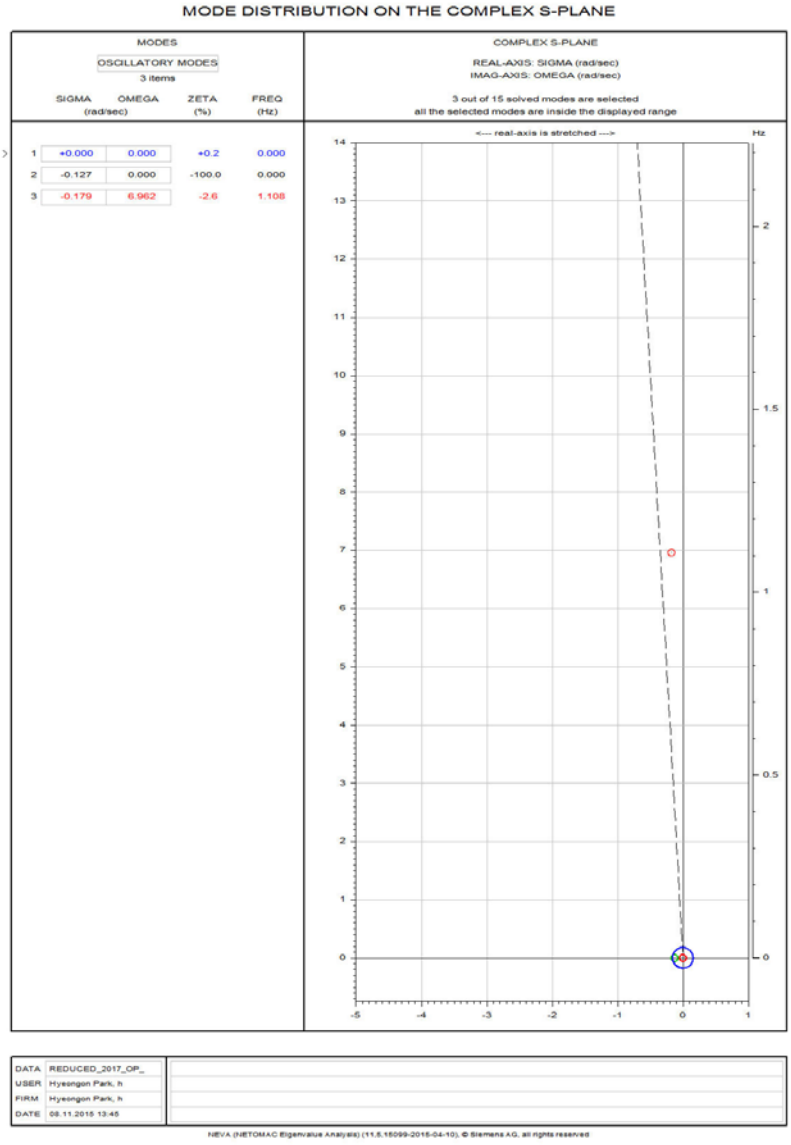

Figure B.1 Operating condition: 0.95 leading for Gen #501

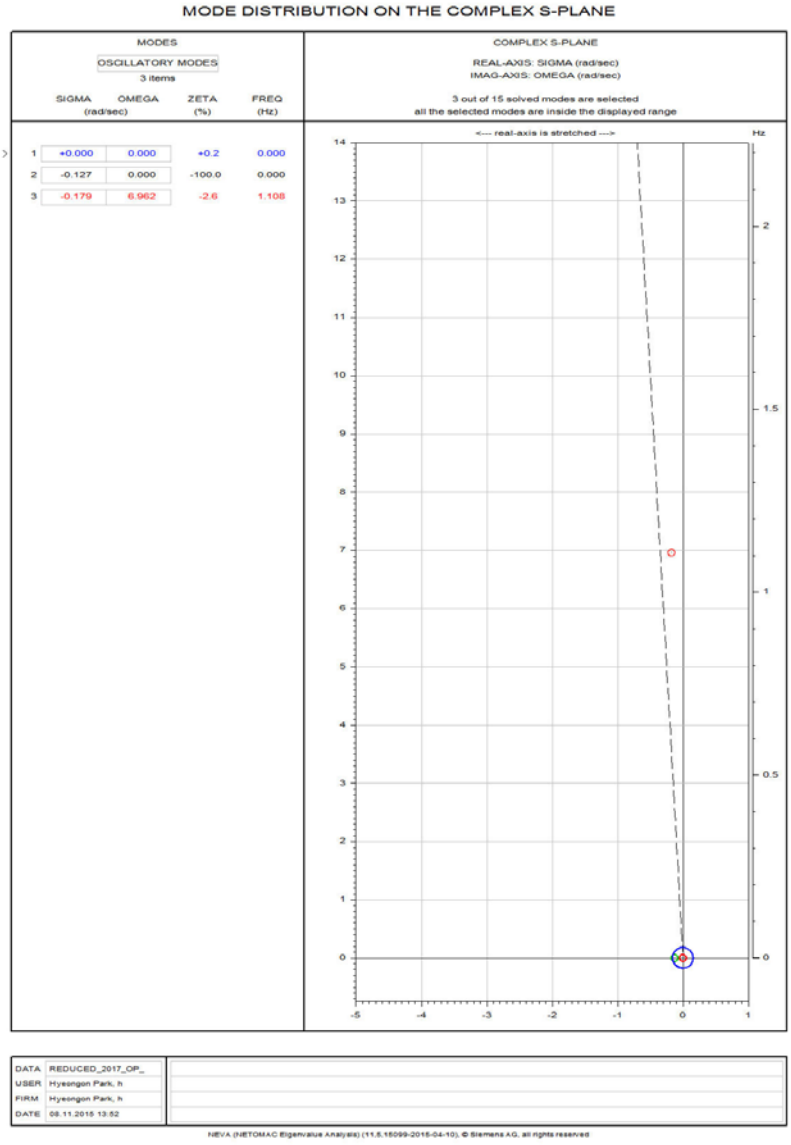

Figure B.2 Operating condition: 0.95 leading for Gen #502

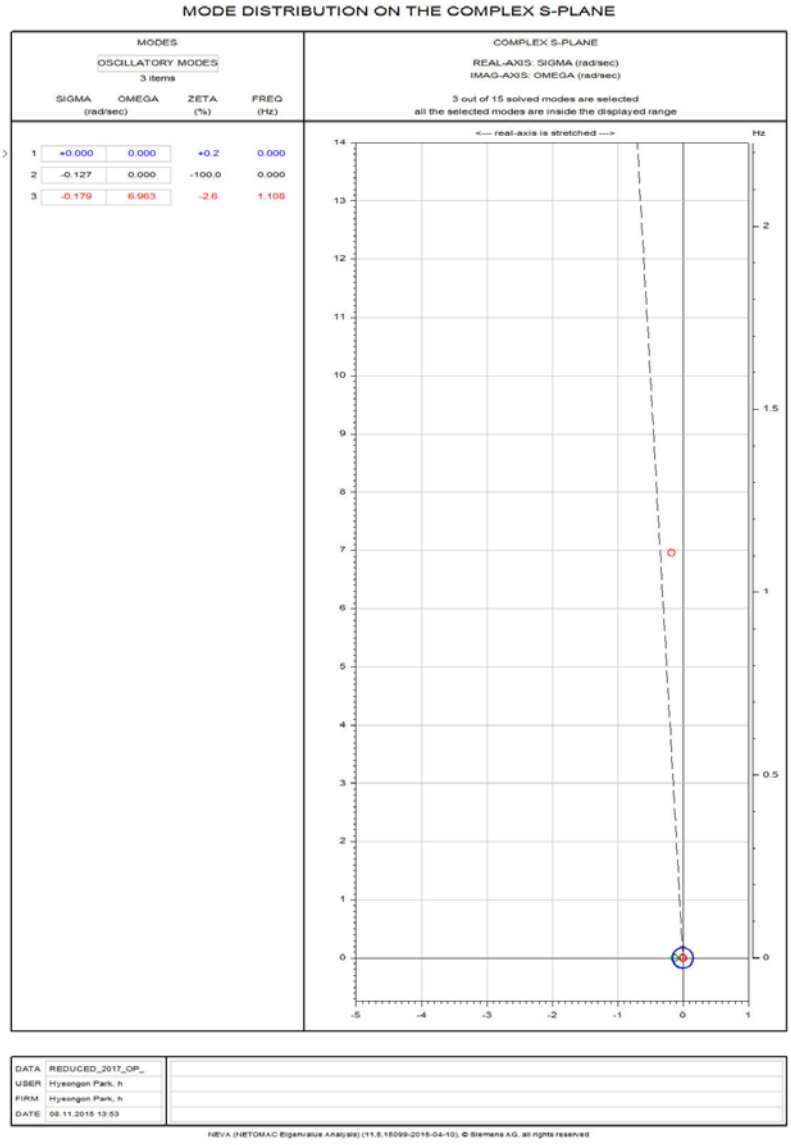

Figure B.3 Operating condition: 0.95 leading for Gen #504

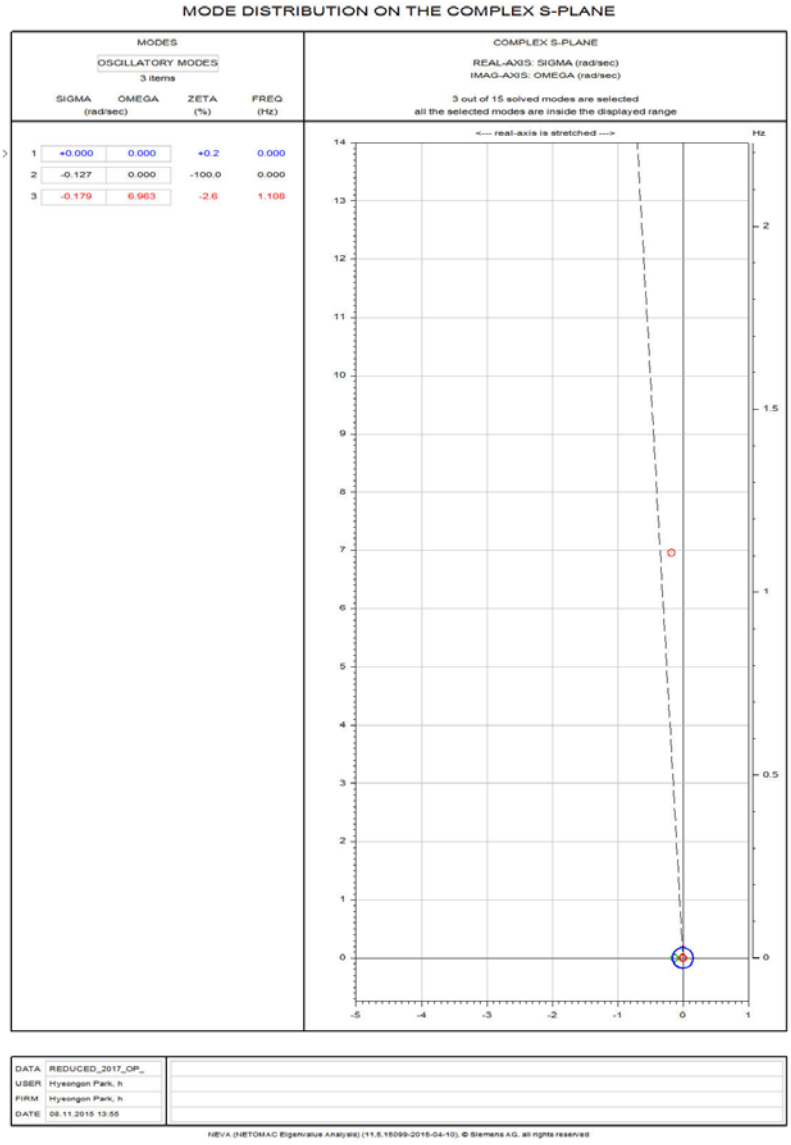

Figure B.4 Operating condition: 0.95 leading for Gen #505

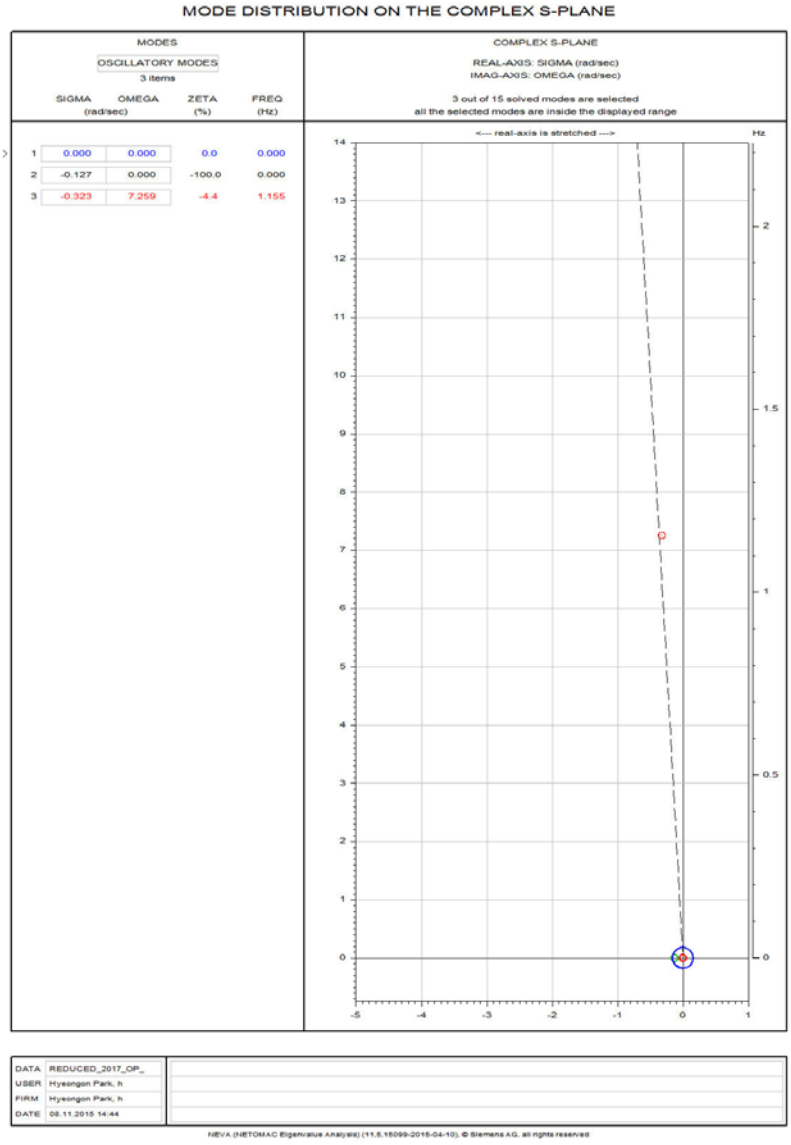

Figure B.5 Operating condition: 0.99 leading for Gen #501

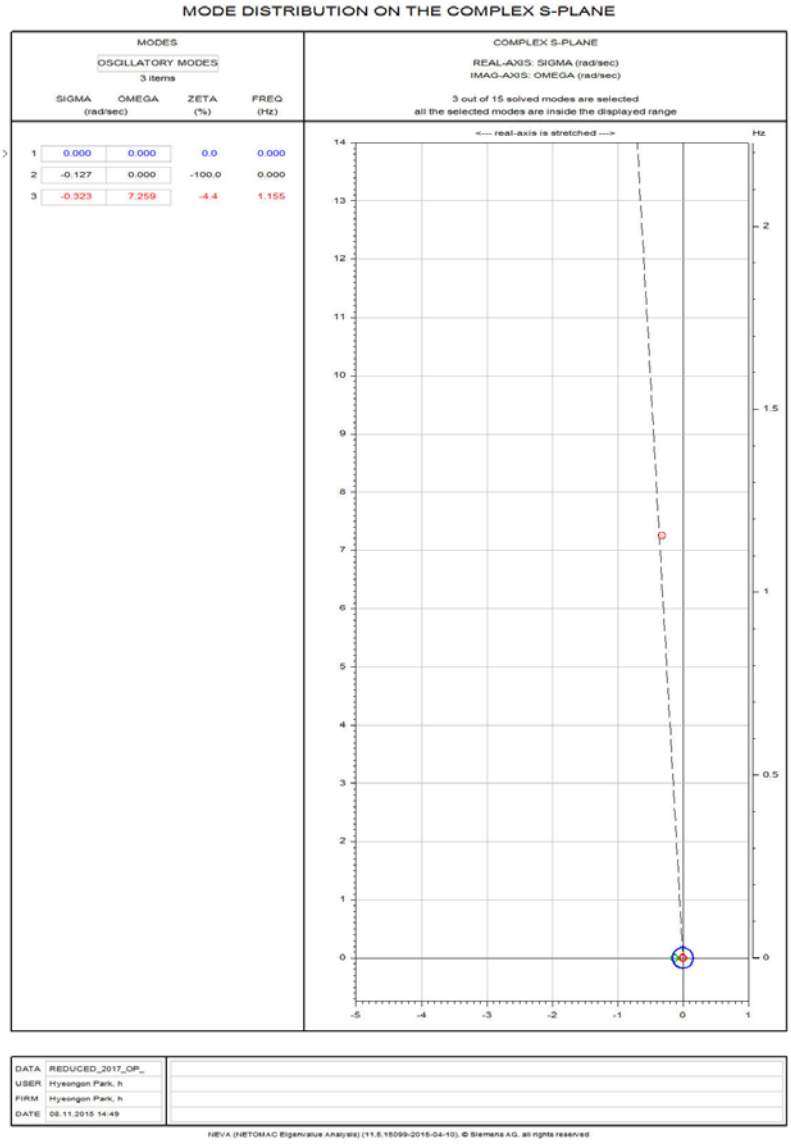

Figure B.6 Operating condition: 0.99 leading for Gen #502

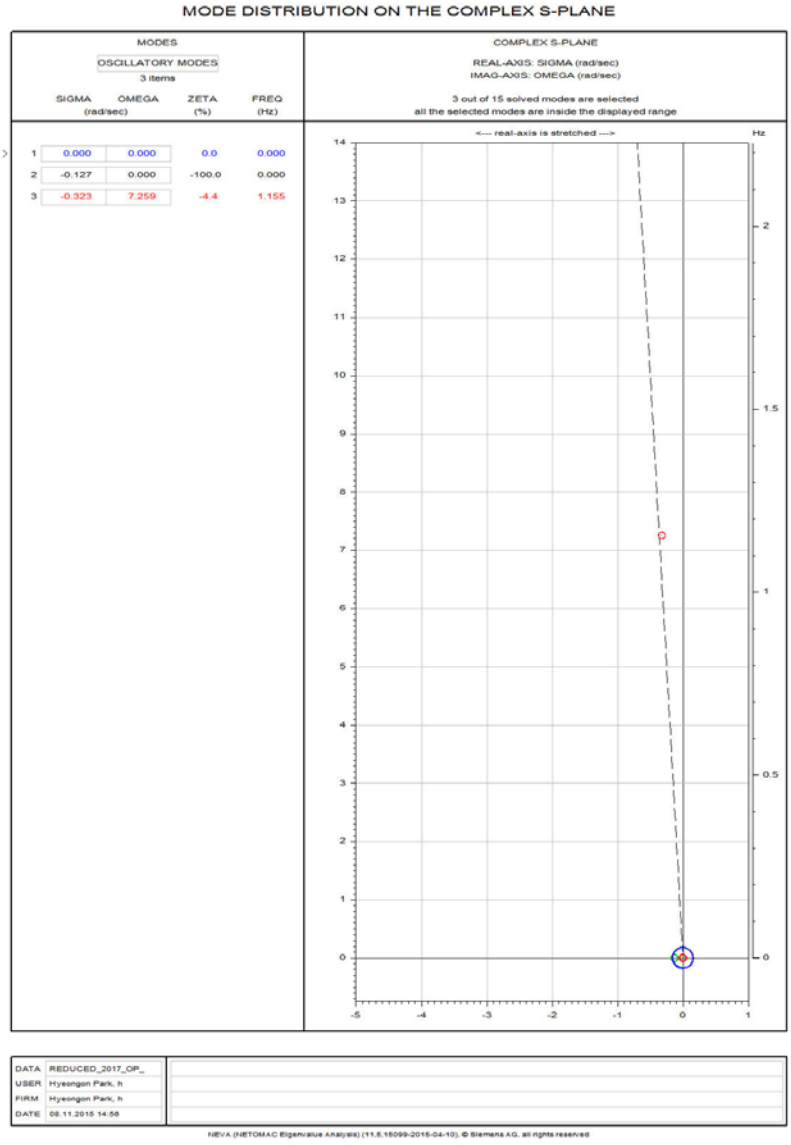

Figure B.7 Operating condition: 0.99 leading for Gen #504

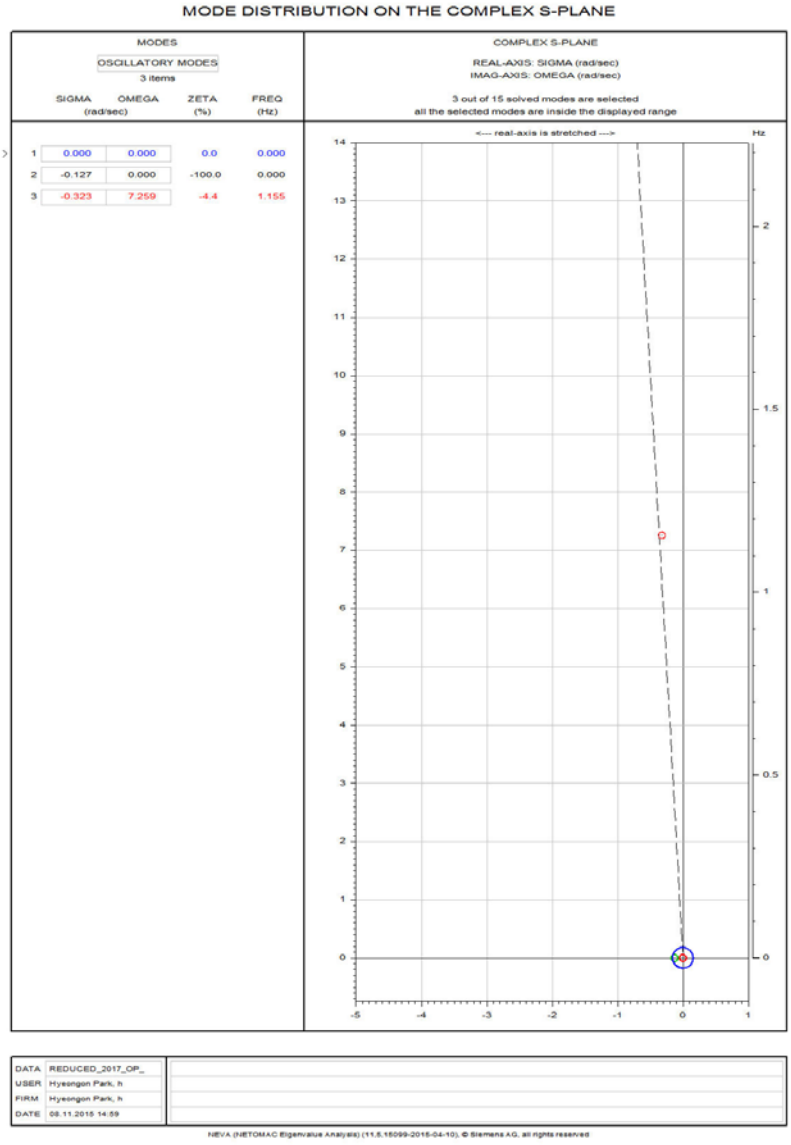

Figure B.8 Operating condition: 0.99 leading for Gen #505

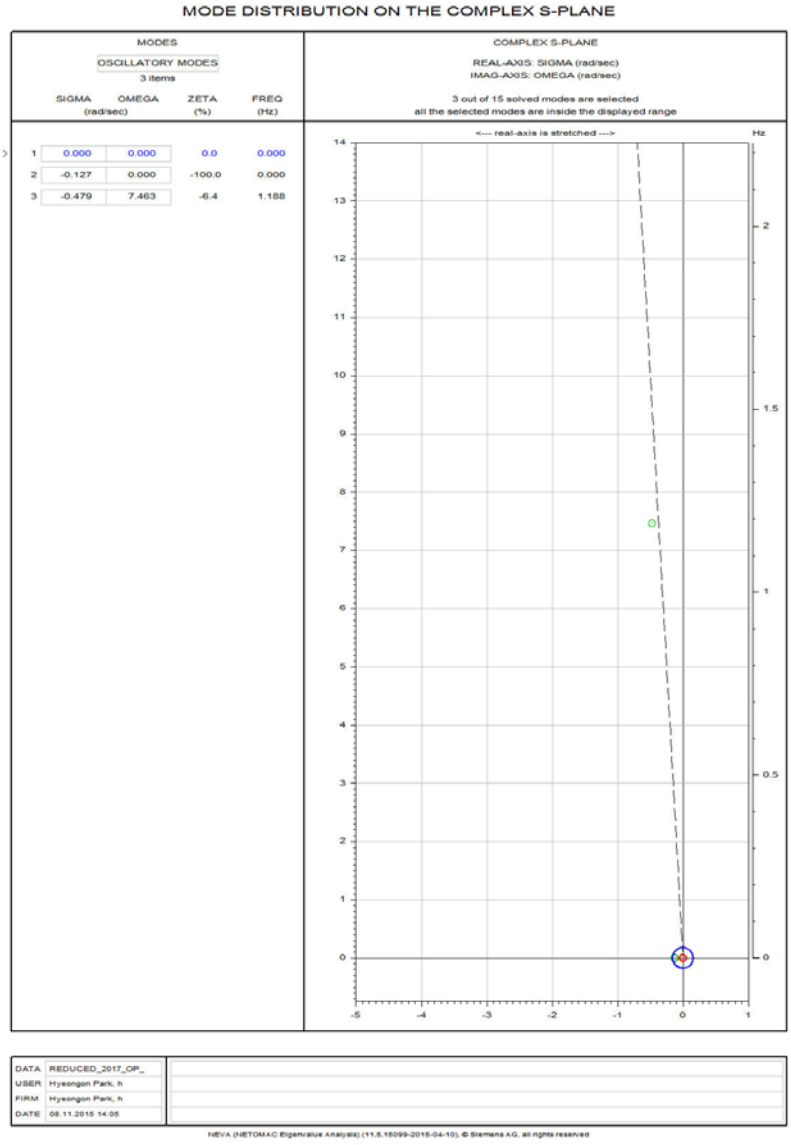

Figure B.9 Operating condition: unity for Gen #501

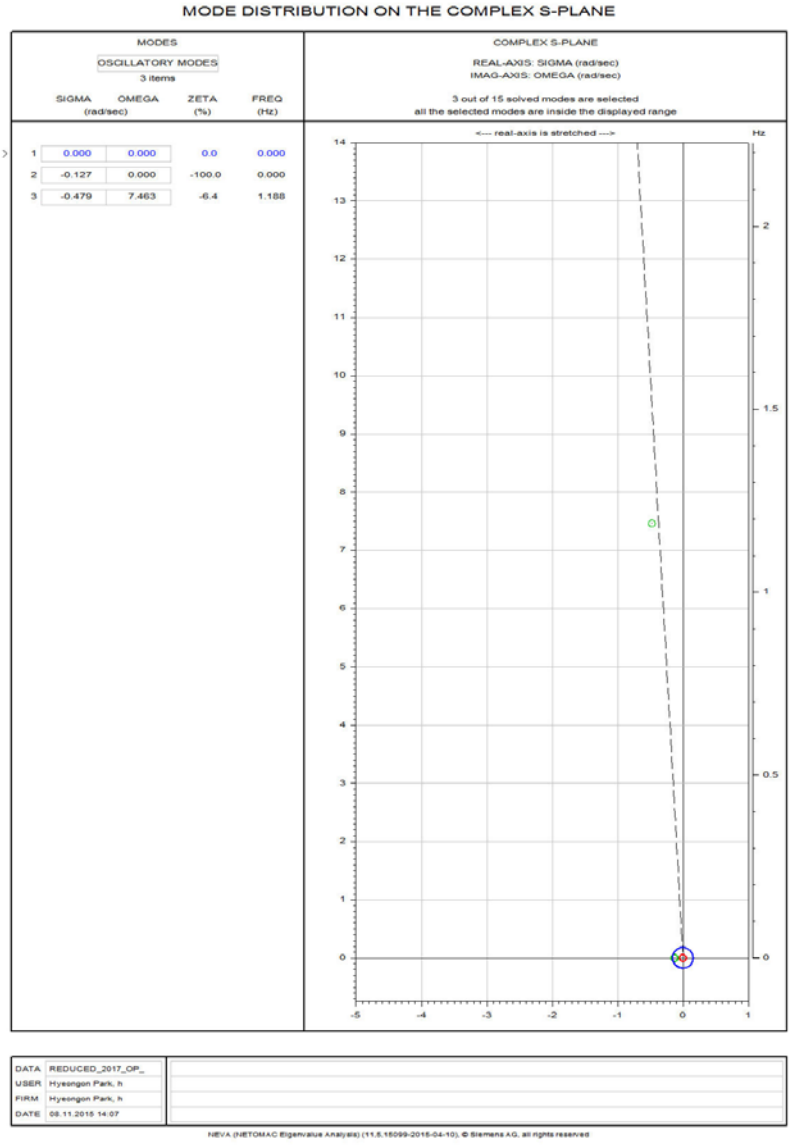

Figure B.10 Operating condition: unity for Gen #502

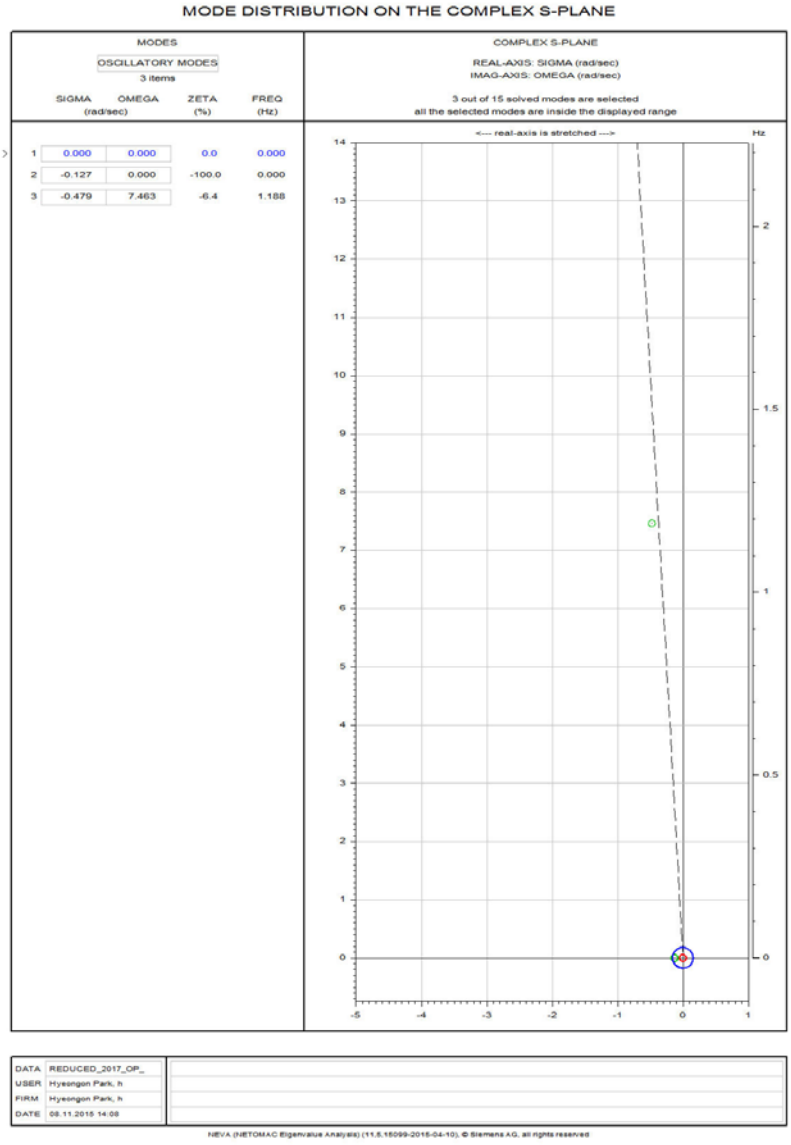

Figure B.11 Operating condition: unity for Gen #504

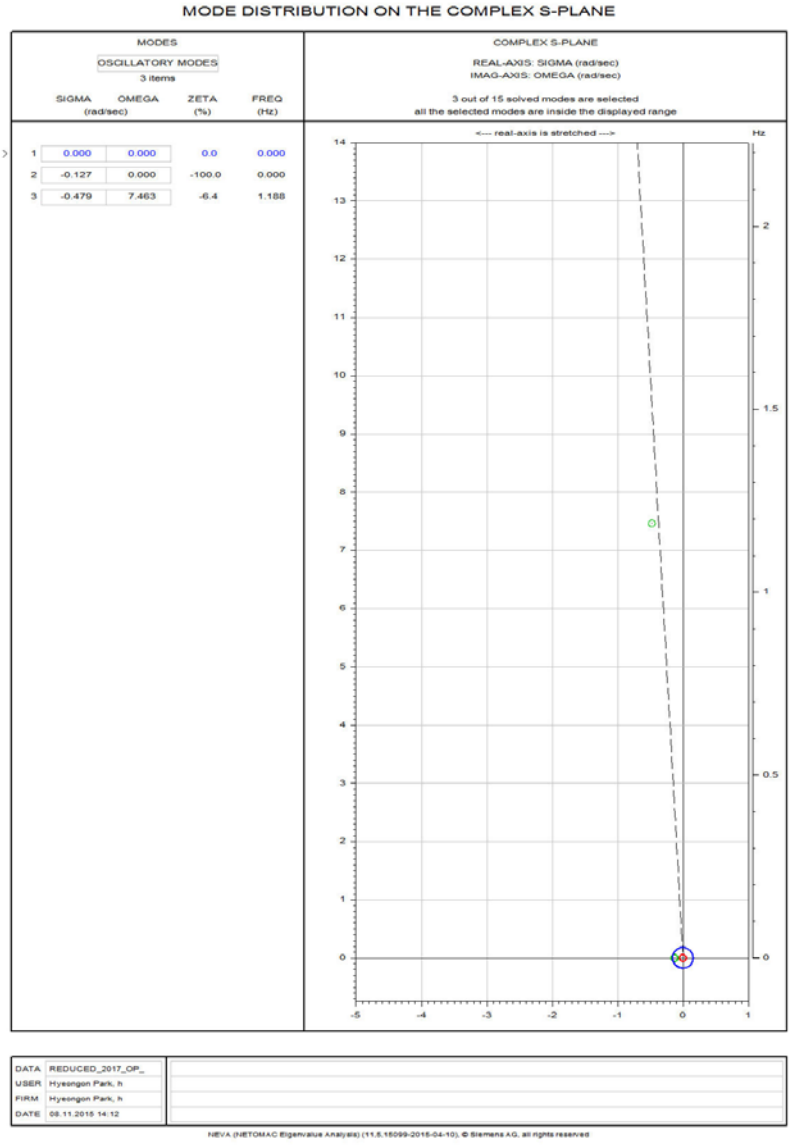

Figure B.12 Operating condition: unity for Gen #505

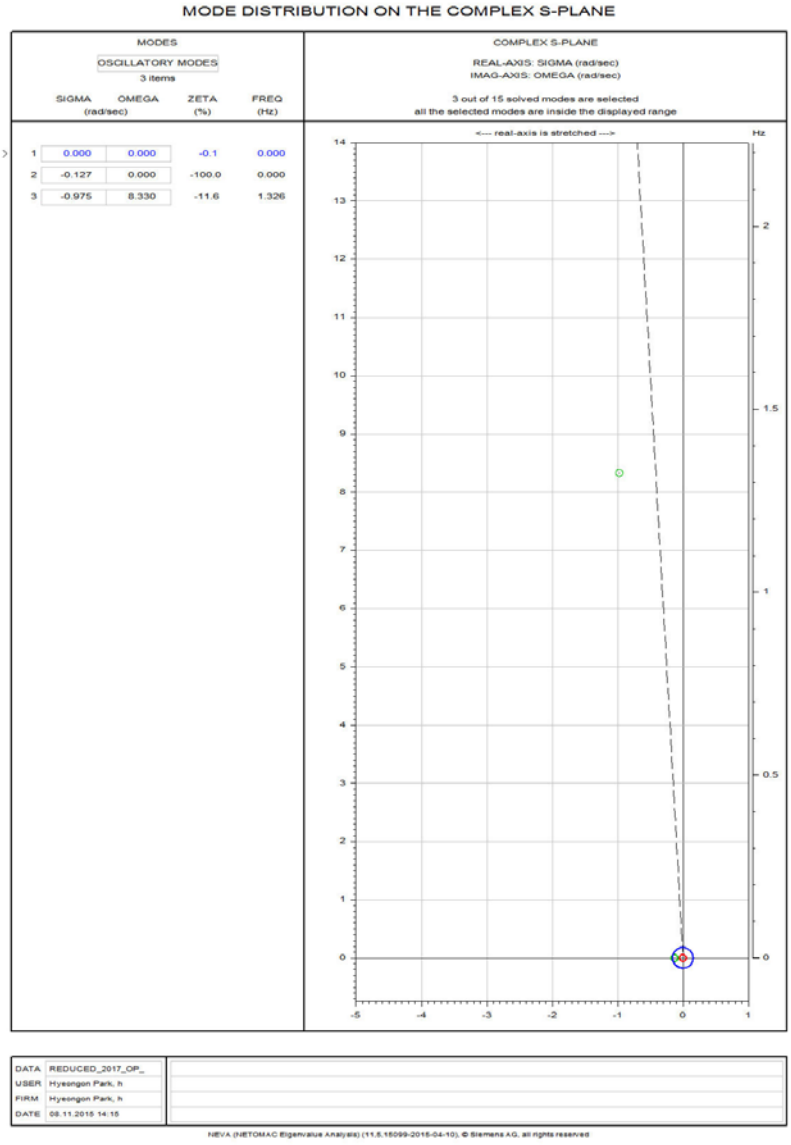

Figure B.13 Operating condition: 0.8 lagging for Gen #501

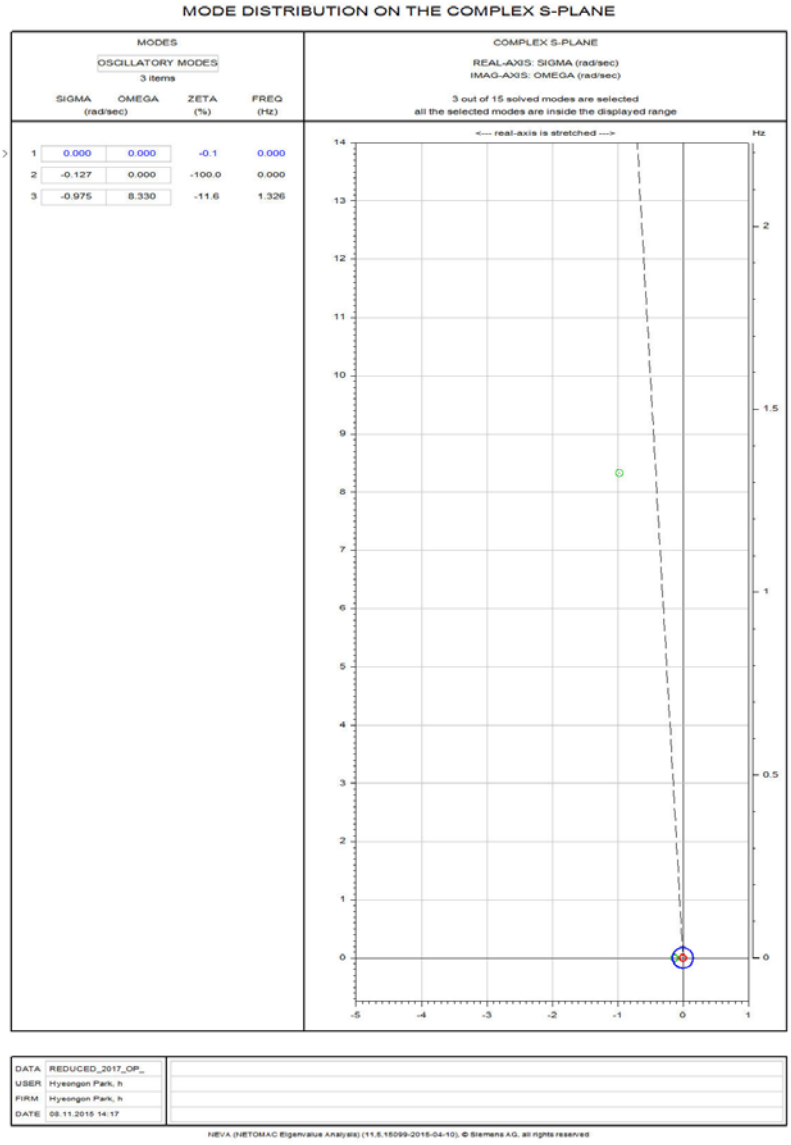

Figure B.14 Operating condition: 0.8 lagging for Gen #502

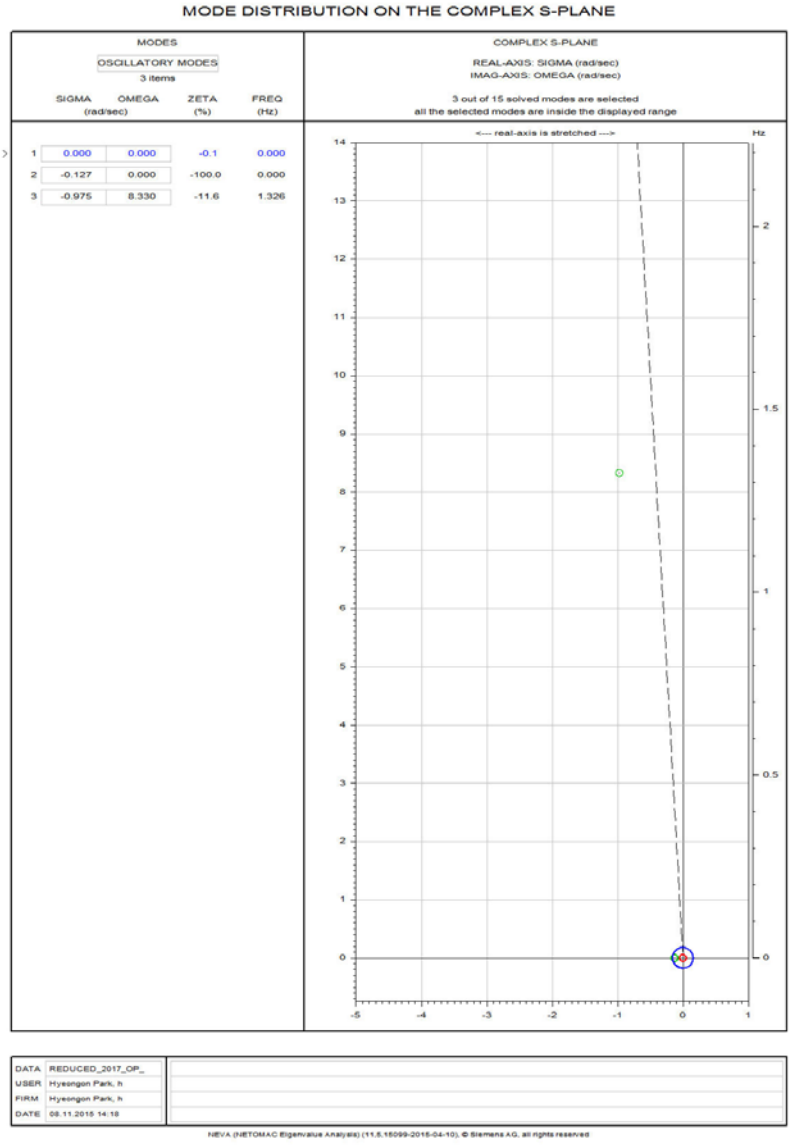

Figure B.15 Operating condition: 0.8 lagging for Gen #504

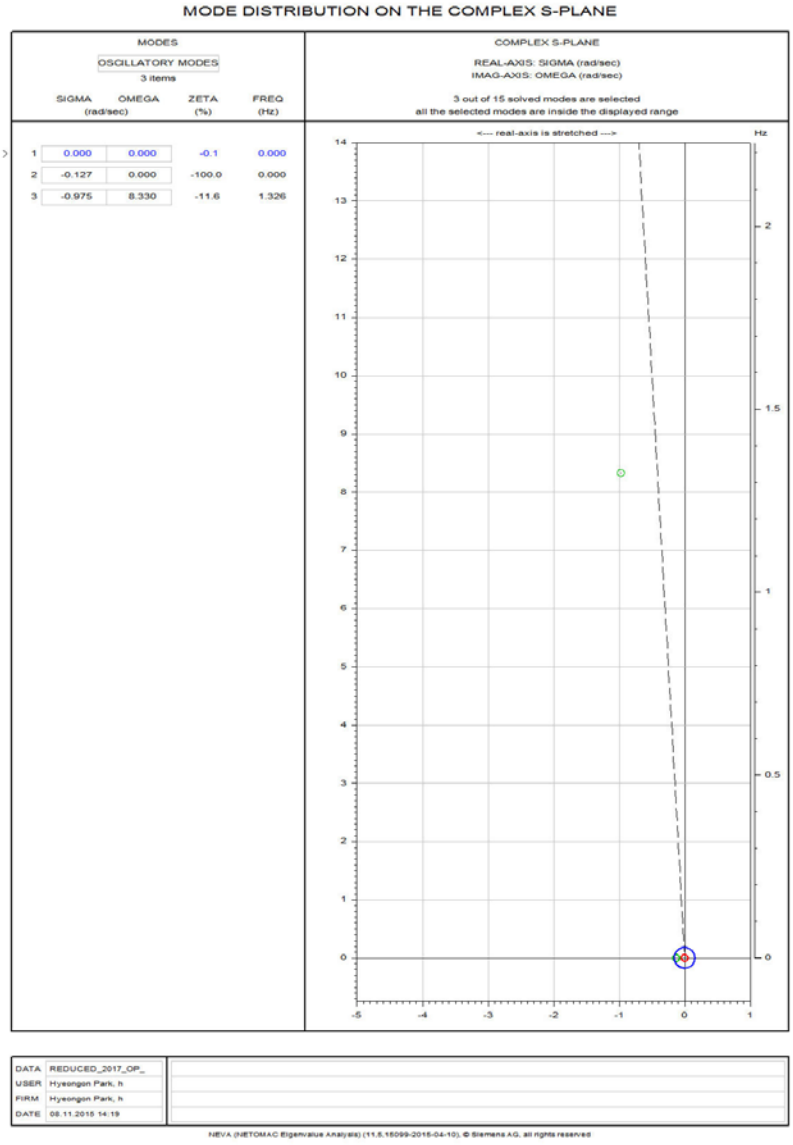

Figure B.16 Operating condition: 0.8 lagging for Gen #505

국문 초록

발전기의 운전조건에 따른 감쇠비의 영향 분석

Jaeyong Kim (김재용)
서울 대학교
전기 정보부

끊임없는 부하나 발전의 변동은 전력 계통에 미소외란을 유발시킨다. 외란이 가해진 후 운전 상태는 평형상태로 옮겨 가기 위해 평형점을 중심으로 해서 상차각이 동요하게 된다. 이때 만약 댐핑이 충분하지 못해 미소외란이 적절히 억제되지 못하고 진동의 크기가 계속 증가하거나 무한히 지속되게 된다면, 동기기는 동기를 잃고 계통은 불안정하게 된다. 오늘날 실제 전력 계통에 있어 미소외란은 주로 계통의 진동에 대한 불충분한 댐핑에 기인한다. 따라서 댐핑을 효율적으로 향상시키는 것이 중요한 관건이다. 본 논문에서는 이론에 기초하고 그것의 사례연구를 통하여 발전기의 운전 조건에 의한 댐핑의 영향을 분석하고자 한다.

미소신호 안정도는 미소외란 아래서 진동이 지속되지 않고 동기를 유지하는 능력을 일컫는다. 따라서 미소외란이 전력계통에 미치는 영향을 알아보기 위해서는 미소신호 안정도 분석이 필수적이다. 이를 위해서는 동기기 역학에 관한 이해를 필요로 한다. 동기기 역학에 관한 식은 발전기 동요방정식으로부터 유도되고 선형화를 거쳐, 상태행렬을 포함한 상태공간식으로 나타낼 수 있다. 고유치와 감쇠비는 이 상태행렬(A행렬)을 가지고 구할 수 있다. 미소신호 분석은 고유치를 이용한 모드 해석 기법을 통하여 해석된다.

한편, 동기 발전기의 가능출력은 발전기가 과열되지 않고 안정적으로 작동할 수 있도록 유효전력과 무효전력의 최대 및 최소 한계치로 형성된 곡선에 의해 모델링된다. 따라서 가능출력 곡선내에 존재하는 점들이 발전기의 안전한 운전점 범위이다. 이 점들이 위치한 지역의 위치에 따라 발전기의 운전점은 진상, 지상, 단일 역률로 나타낸다.

동기 토크 계수 및 댐핑 토크 계수의 관계식은 발전기의 진상, 지상 혹은 단일 역률의 운전 조건에 관해서 나타낼 수 있다. 동기 및 댐핑 토크 계수를 구하기 위해 필수적인 무한모선 전압식은 단순 네트워크 계통의 전압 관계식으로부터 유도된다. 본 연구에서는 감쇠비와 동기 및 댐핑 토크 계수 간의 수학적 선형 관계를 살펴 보았다. 동기 토크 계수의 증가는 비감쇠 고유

진동수의 증가를 가져온다. 반면 댐핑 토크의 증가는 댐핑을 향상시킨다.

댐핑에 대한 발전기 운전조건의 영향이 PSS/E 소프트웨어를 이용하여 1기 무한 모선을 가지고 모의 되었다. 그런 다음 이를 실제계통에 확대 적용하였다. 이론의 검증을 위하여 페르시아 걸프지역의 특정 발전기들이 선택되었고, 고유치를 구하여 복소 S평면상에 표시하였다. 진상에서 단일, 그리고 지상으로 갈수록 감쇠비가 향상됨이 확인되었다. 대부분의 모드가 안전 영역에 위치하였고 따라서 전력계통의 미소신호 안정도를 확신하기 위한 조건을 만족하였다. 이 모의를 통해 더 나은 댐핑을 위해 발전기의 운전조건이 고려되어야 함을 확인 할 수 있었다.

본 논문에서 감쇠비에 대한 발전기의 운전 조건의 영향이 평가되었다. 감쇠비에 대한 이론적 관계식과 사례연구 모의 결과 모두 발전기의 운전조건 변화가 감쇠비에 영향을 끼침을 보여주었다. 따라서 전력 계통의 감쇠비 향상을 위해서는 제어기의 성능 뿐만 아니라 발전기의 운전 조건 또한 고려되어야 할 것이다.

주요어: 감쇠비, 미소 신호 안정도, 운전 조건, 댐핑 토크 계수, 동기 토크 계수, 출력 한계 곡선

학 번: 2015-20906